



Understanding and improving model representation of aerosol optical properties for a Chinese haze event measured during KORUS-AQ

Pablo E. Saide^{1,2}, Meng Gao³, Zifeng Lu⁴, Dan Goldberg⁴, David G. Streets⁴, Jung-Hun Woo⁵, Andreas Beyersdorf⁶, Chelsea A. Corr⁷, Kenneth L. Thornhill⁸, Bruce Anderson⁸, Johnathan W. Hair⁸, Amin R. Nehrir⁸, Glenn S. Diskin⁸, Jose L. Jimenez⁹, Benjamin A. Nault⁹, Pedro Campuzano-Jost⁹, Jack Dibb¹⁰, Eric Heim¹⁰, Kara D. Lamb¹¹, Joshua P. Schwarz¹¹, Anne E. Perring¹², Jhoon Kim¹³, Myungje Choi^{13,14}, Brent Holben¹⁵, Gabriele Pfister¹⁶, Alma Hodzic¹⁶, Gregory R. Carmichael¹⁷, Louisa Emmons¹⁶, and James H. Crawford⁸

¹Department of Atmospheric and Oceanic Sciences, University of California – Los Angeles, Los Angeles, CA, USA

²Institute of the Environment and Sustainability, University of California – Los Angeles, Los Angeles, CA, USA

³Department of Geography, Hong Kong Baptist University, Hong Kong SAR, China

⁴Energy Systems Division, Argonne National Laboratory, Argonne, IL 60439, USA

⁵Department of Technology Fusion Engineering, Konkuk University, Seoul, South Korea

⁶Department of Chemistry & Biochemistry, California State University San Bernardino, San Bernardino, CA, USA.

⁷USDA UV-B Monitoring and Research Program, Natural Resource Ecology Laboratory, Colorado State University, Fort Collins, CO, USA.

⁸NASA Langley Research Center, Hampton, VA, USA

⁹Department of Chemistry, and Cooperative Institute for Research in Environmental Sciences, University of Colorado, Boulder, CO, USA

¹⁰Institute for the Study of Earth, Oceans, and Space, University of New Hampshire, Durham, NH, USA

¹¹Earth System Research Laboratory, NOAA, Boulder, CO, USA

¹²Department of Chemistry, Colgate University, Hamilton, NY, USA

¹³Department of Atmospheric Sciences, Yonsei University, Seoul, 120-749, Korea

¹⁴NASA Jet Propulsion Laboratory, Pasadena, California, USA.

¹⁵NASA Goddard Space Flight Center, Greenbelt, Maryland, USA.

¹⁶Atmospheric Chemistry Observations and Modeling Lab, National Center for Atmospheric Research, Boulder, CO, USA

¹⁷Center for Global & Regional Environmental Research, University of Iowa, Iowa City, Iowa, USA

Correspondence to: Pablo E. Saide (saide@atmos.ucla.edu)

Abstract. KORUS-AQ was an international cooperative air quality field study in South Korea that measured local and remote sources of air pollution affecting the Korean peninsula during May-June 2016. Some of the largest aerosol mass concentrations were measured during a Chinese haze transport event (May 24th). Air quality forecasts using the WRF-Chem model with aerosol optical depth (AOD) data assimilation captured AOD during this pollution episode but over-predicted surface particulate matter concentrations, especially PM_{2.5} often by a factor of 2 or larger. Analysis revealed multiple sources of model deficiency related to the calculation of optical properties from aerosol mass that explain these discrepancies. Using in-situ observations of aerosol size and composition as inputs to the optical properties calculations showed that using a low resolution size bin representation under-estimates the efficiency at which aerosols scatter and absorb light (mass extinction



efficiency). Besides using finer-resolution size bins, it was also necessary to increase the refractive indices and hygroscopicity of select aerosol species within the range of values reported in the literature to achieve consistency with measured values of mass/volume extinction efficiencies and light scattering enhancement factor ($f(\text{RH})$) due to aerosol hygroscopic growth. Furthermore, evaluation of optical properties obtained using modeled aerosol properties revealed the inability of sectional and modal aerosol representations in WRF-Chem to properly reproduce the observed size distribution, with the models displaying a much wider accumulation mode. Other model deficiencies included an under-estimate of organic aerosol density and an over-prediction of the fractional contribution of inorganic aerosols other than sulfate, ammonium, nitrate, chloride and sodium (mostly dust). These results illustrate the complexity of achieving an accurate model representation of optical properties and provide potential solutions that are relevant to multiple disciplines and applications such as air quality forecasts, health-effect assessments, climate projections, solar-power forecasts, and aerosol data assimilation.

1. Introduction

Exposure to air pollutants is estimated to be the leading environmental risk affecting human health (Gakidou et al., 2017) and aerosols represent the leading pollutant responsible for these effects (Cohen et al., 2017). The estimates of aerosol impacts on human health generally involve the use of ground-based monitoring networks that are combined with aerosol optical depth (AOD) satellite retrievals and/or model estimates for regions not monitored to obtain global estimates (Liu et al., 2009; van Donkelaar et al., 2016; Goldberg et al., 2019a). The use of AOD to estimate surface concentrations often involves using atmospheric composition simulations able to “translate” a column-integrated measure of light extinction due to aerosols (AOD) into surface aerosol mass concentrations. Satellite AOD is also often used to improve air quality forecasts of surface particulate matter through data assimilation (Saide et al., 2013; Saide et al., 2014; Kumar et al., 2019; Benedetti et al., 2009). Aerosols also impact climate through aerosol-cloud-radiation interactions and represent one of the largest uncertainties in climate projections (Boucher et al., 2013). Chemistry-climate models estimate 3-D distributions of aerosols, which are used by the radiative transfer module to estimate aerosol radiative effects. Again, this translation of aerosol mass to optical properties is performed in these models, often showing large inter-model variability (Myhre et al., 2013; Stier et al., 2013). Similarly, short term predictions of solar power (Schroedter-Homscheidt et al., 2013; Jimenez et al., 2016) and visibility forecasts (Clark et al., 2008; Lee et al., 2016a) also require the use of aerosol optical properties. Thus, evaluating the ability of models to properly translate aerosol mass and number concentrations into aerosol optical properties is key to providing confidence in model results supporting these disciplines.

Previous research has shown various degrees of consistency between model evaluations of surface aerosol mass concentrations and column integrated aerosol properties. Lee et al. (2016b) used satellite AOD to constrain surface PM_{10} (particulate matter with diameters below $10\ \mu\text{m}$) predictions and found large improvements against surface monitors regardless of the aerosol optical properties model used. Their results also showed slight discrepancies in the PM_{10} and AOD



70 when comparing models to observations, with some optical models showing larger biases in PM_{10} than AOD and some
presenting the opposite behavior. Lennartson et al. (2018) also found discrepancies when comparing the ratio between $PM_{2.5}$
and AOD for observations and WRF-Chem simulations, finding the modeled ratios were 30-50% higher over South Korea
during May-June 2016. Similar discrepancies were found by Mangold et al. (2011) when assessing model skill in predicting
75 an ensemble of simulations to assess what combination of model inputs and configurations resulted in the best agreement to
observations in the southeast US. They reported that simulations configured with a modal aerosol model performed the best
against AOD observations, while a sectional aerosol approach showed the best agreement against surface $PM_{2.5}$,
hypothesizing that aerosol hygroscopic growth and optical properties calculations could play a role in this discrepancy.
Reddington et al. (2016) evaluated a global aerosol model in tropical regions affected by biomass burning. They found that
80 the model under-estimated AOD more than $PM_{2.5}$, even when an upper limit estimate of aerosol hygroscopicity was assumed
for the aerosols. Reddington et al. (2019) found further inconsistencies, as the model showed good representation of
observed vertical profile while under-estimating AOD and hypothesized it was due to uncertainties in the AOD
computations. In another study, Zieger et al. (2013) compared observations of scattering enhancement due to hygroscopic
growth against results from the Optical Properties of Aerosols and Clouds (OPAC) software module showing a systematic
85 over-prediction. This over-prediction could lead to mismatches between AOD and $PM_{2.5}$ in models using this code.
KORUS-AQ (KOREan United States Air Quality) Campaign was an international cooperative air quality field study in South
Korea that measured local and remote (e.g., anthropogenic, biomass burning, dust) sources of air pollution affecting the
Korean peninsula during May-June 2016. The objectives of the present study are to: 1) Evaluate one of the forecast system
used to support flight planning during the mission; 2) Assess the degree of consistency between aerosol optical properties
90 and mass concentrations for the forecasting and other configurations; and, 3) Explain the identified discrepancies. The results
will provide guidance to future model development and we expect will motivate this type of analysis for other modeling
systems and locations.

2. Methods

2.1 Regional modeling

95 Air quality forecasts were performed using the Weather Research and Forecasting model (Skamarock et al., 2008) coupled to
Chemistry (WRF-Chem) (Grell et al., 2005) to support both KORUS-AQ flight planning and post-campaign analysis. The
modeling domains are shown in Figure 1, with a regional domain of 20 km resolution, covering major source regions of
transboundary pollutants affecting the Korean Peninsula: anthropogenic pollution from eastern China, dust from inner China
and Mongolia, and wild fires from Siberia (Saide et al., 2014). A 4 km resolution domain was nested to cover the Korean
100 Peninsula and surroundings at higher resolution. This inner domain encompassed the region where the KORUS-AQ flights
were planned and was able to better resolve local sources. Anthropogenic emissions were developed by Konkuk University



for KORUS-AQ forecasting and are described in Choi et al. (2019a) and Goldberg et al. (2019b) . The forecasts were performed once daily and used meteorological initial and boundary conditions from National Centers for Environmental Prediction Global Forecast System (NCEP, 2007) and chemical boundary conditions from the Copernicus Atmosphere Monitoring Service (Inness et al., 2015). Initial conditions for gases and aerosols were obtained from the previous forecasting cycle. AOD data assimilation was implemented for the outer domain using data from low-earth orbiting (GMAO Neural Network retrieval) and geostationary satellites (Geostationary Ocean Color Imager retrievals (Choi et al., 2018; Choi et al., 2016)) as described in Saide et al. (2014). To our knowledge, this was the first near-real time implementation of assimilating geostationary AOD. Each assimilation step modified aerosol mass keeping the species distribution and size of each bin constant. Thus, the assimilation had the potential to change the bin-aggregated composition and size distribution when size bins with different composition were scaled differently. Although there was no data assimilation performed on the inner domain, this domain was initialized 18 hours after the outer domain and thus was influenced by data assimilation through initial and boundary conditions. The forecast configuration was based on WRF-Chem version 3.6.1 with modifications. The aerosol and gas-chemistry packages corresponded to the 4-size bin Model for Simulating Aerosol Interactions and Chemistry (MOSAIC, Zaveri et al., 2008) and a simplified hydrocarbon chemical mechanism (Pfister et al., 2014), both selected to reduce computational costs compared to using the 8 size bin MOSAIC configuration and more complex chemical mechanisms. Although detailed secondary organic aerosol (SOA) formation schemes have been implemented for the 4-bin MOSAIC configuration (Shrivastava et al., 2013; Knote et al., 2015), it increases computational costs significantly. Thus, the simplified SOA formation scheme, proposed by Hodzic and Jimenez (2011) and verified to work well in multiple later studies (e.g., Hayes et al., 2015; Shah et al., 2019), was implemented to keep computational costs low. While this scheme included anthropogenic and biomass burning SOA, biogenic SOA was also modeled by using a SOA precursor surrogate derived from isoprene as described in Shrivastava et al. (2011). Other modeling configurations related to meteorological parametrizations, analysis nudging, and other emission sources are described in Saide et al. (2014).

In addition to the forecasting results, we performed retrospective sensitivity simulations summarized in Table 1. We first used the same configuration as the forecast, which we labeled MOSAIC4b. To explore the model sensitivity to increasing the resolution of the aerosol size bins, we performed simulations using the MOSAIC 8-bin configuration, coupled to the Carbon-Bond Mechanism version Z (CBM-Z) chemical scheme (Zaveri and Peters, 1999). Some caveats of this sensitivity simulation are that it uses a different gas-phase chemistry scheme and does not include secondary organic aerosol formation, thus this needs to be considered in the analysis when comparing it to the base configuration. This simulation is labeled MOSAIC8b. WRF-Chem can also be configured with the Modal Aerosol Dynamics Model for Europe (MADE) model, where aerosol sizes are represented by log-normal modes (as opposed to sections as for MOSAIC). We used the configuration coupled to the updated Regional Atmospheric Chemistry Mechanism (RACM, Ahmadov et al., 2014) which contains secondary organic aerosol formation using the volatility basis-set (Ahmadov et al., 2012) and aerosol optical properties calculations (Tuccella et al., 2015). We label these simulations as RACM#, with # going from 1-4 depending on changes to parameters described in Table 1.



Simulations MOSAIC4b, MOSAIC8b and RACM1 are referred to as base configurations, while RACM2-4 are sensitivity simulations. All retrospective simulations were performed only for the 20 km resolution domain in this study, as we focus on a pollution event from long range transport. Also, no data assimilation was performed for these simulations. Unless otherwise noted, they use the same inputs and parametrizations as for the forecast simulations.

140 2.2 Optical properties calculation

Aerosol optical properties in WRF-Chem are computed using a Mie code and Chebyshev expansion coefficients for each size bin, assuming an internal mixture within the bin and a volume mixing rule (Fast et al., 2006). The refractive indices (real part) and density used for each species are defined in Table 2 under the base configuration column. Only black carbon and other inorganics (OIN, inorganic aerosols other than sulfate, ammonium, nitrate, chloride and sodium) are considered to
145 absorb solar radiation with an imaginary refractive index of 0.71 and 0.006, respectively. For the MOSAIC configurations, the size bins in the optical properties calculation correspond to those in the aerosol model (4 and 8 size bins, defined in Table 3); while, for modal aerosols, the modes are mapped to 8 sectional bins (same boundaries as the MOSAIC 8 bins) before the calculation by computing the aerosol mass and number concentration included in each section. WRF-Chem computes optical properties for ambient conditions. Thus, derivation of dry-extinction and scattering enhancements due to hygroscopic growth
150 at fixed relative humidity require off-line computations. These computations require the aerosol water to be recalculated for the specified relative humidity. Since both the MOSAIC and MADE aerosol models compute aerosol water based on aerosol thermodynamics, off-line versions of these computations are needed. In order to simplify the process and add additional capabilities, an alternative off-line optical properties code was developed that mimics the WRF-Chem one. This alternative approach uses Mie calculations from Mätzler (2002) code which is based on the Appendix of Bohren and Huffman (1983).
155 Aerosol water uptake was parameterized using the method proposed by Petters and Kreidenweis (2007), which utilizes the hygroscopicity parameter (κ). Values for the hygroscopicity parameter representing the base configuration are obtained from the WRF-Chem code used to compute aerosol water for the Goddard Chemistry Aerosol Radiation and Transport (GOCART, Chin et al., 2002) model which implements the κ approach and a volume mixing rule. Following this configuration κ is set to 0.5 for ammonium sulfate and ammonium nitrate, and 1.16 for sodium chloride. For organic
160 aerosol, black carbon, and dust, κ is set to zero as these aerosol types are currently not considered as electrolytes in the MOSAIC and MADE thermodynamic models and thus do not contribute to water uptake in these frameworks (Fast et al., 2006). Ways to improve these simplifications will be discussed later in the text. Figure 2 shows an evaluation of the alternative approach against the off-line WRF-Chem routines for the MOSAIC model that were developed as part of the data assimilation scheme (Saide et al., 2013). Under dry conditions, the alternative approach shows similar results as the WRF-
165 Chem optical properties with the extinction to mass ratio curve, following each other for all sizes (Fig. 2a). The high frequency oscillations shown by the Mie code of our alternative approach are smoothed in WRF-Chem due to the use of the Chebyshev expansion coefficients (Fast et al., 2006) and interpolation between wavelengths (optical properties at 400 nm and 600 nm are used to derive values at mid-visible wavelengths). Water uptake using the MOSAIC approach and the one



described here provides similar results (Fig 2b), with values ~10% lower in the alternative approach that will be taken into
170 consideration when evaluating the optical properties code in the next sections. The alternative optical properties code
provides flexibility to evaluate changes in configuration that would be difficult to implement in the WRF-Chem optical
properties code. These include using more than 8 bins to improve size resolution, using variable density for aerosol species,
and altering κ to vary the extent that different aerosol chemical species take up water.

2.3 Airborne Observations

175 Airborne data used in this study were obtained on the NASA DC-8 during the KORUS-AQ campaign (Aknan and Chen,
2019) during the flight starting at 22:00 UTC on May 24th (May 25th in local Korean time) 2016. This flight focused on
measurements over the Yellow Sea and sampled some of the highest aerosol mass concentrations of the deployment
originating from mostly anthropogenic pollution from China (Peterson et al., under review; Nault et al., 2018) . This flight
was also chosen as it corresponds with a period of large model discrepancies (see Results Section). Measurements used in
180 this study include numerous in-situ chemical composition and mass concentration and physical properties of the aerosol, and
remote sensing physical properties of the aerosol. PM_{10} , not including black carbon, was measured by the University of
Colorado Boulder, High-Resolution Time-of-Flight Aerosol Mass Spectrometer (HR-ToF-AMS, hereinafter “AMS” for
short) (DeCarlo et al., 2006; Nault et al., 2018). These measurements included the mass concentrations of sulfate, nitrate,
ammonium, chloride, and organic aerosol, and the estimated aerosol density. The estimation of aerosol density is described
185 in Nault et al. (2018) and DeCarlo et al. (2004). Refractory black carbon concentrations were measured by the NOAA Single
Particle Soot Photometer (SP2) (Lamb et al., 2018). Bulk water-soluble, inorganic aerosol was measured by the University
of New Hampshire using Teflon filters, followed by off-line ion chromatography with an estimated aerodynamic diameter
cut-off of ~4 μm (SAGA, Dibb et al., 2000; McNaughton et al., 2007). The in-situ, physical aerosol properties were
measured by NASA Langley Aerosol Research Group (LARGE), which included dry aerosol scattering, extinction and
190 single-scattering albedo, and scattering enhancements due to hygroscopic growth. These measurements were done with two
TSI nephelometers (at 450, 550, and 700 nm wavelength) and a Particle Soot Absorption Photometer (at 470, 532, and
660nm wavelength) (Ziemba et al., 2013). Aerosol size distributions were also measured by the LARGE suite using a
Scanning Mobility Particle Sizer (SMPS, TSI model 3936), a Laser Aerosol Spectrometer (LAS, TSI model 3340) and an
Aerodynamic Particle Sizer (APS, TSI model 3321). AMS and SP2 measure mostly submicron aerosols while the LARGE
195 inlet cut-off is at 5 μm aerodynamic diameter (McNaughton et al., 2007). Relative humidity was estimated using
measurements of water vapor from the NASA Langley/Ames Diode Laser Hygrometer (Podolske et al., 2003). Finally,
extinction curtains were measured using the Airborne Differential Absorption Lidar (DIAL) – High Spectral Resolution
Lidar (HSRL) (Hair et al., 2008), from the NASA Langley LIDAR group. In-situ data was obtained from the 1 second
merges (version 3) and merged with the corresponding version of data that was available through individual files (e.g., size
200 distributions).



Though the instruments measuring size distributions overlap in some size bins, they use different sampling frequencies, and they use different sizing techniques based on different measures of aerosol diameters (e.g., geometric, optical and aerodynamic). Thus, these measurements need to be homogenized and combined to obtain a single size distribution. Thirty-two size bins using geometric diameter from a lower bound of 39 nm to an upper bound of 10 μm with a width (dlnD) of 0.1737 are used to re-bin the SMPS, LAS and APS size distributions. These boundaries and width are chosen so the distributions can be easily aggregated to the modeled size bins (Table 3). Data from the SMPS, LAS and APS are used for bins 1-8 (39 nm – 156 nm), 9-18 (156 nm- 743 nm) and 19-32 (743 nm – 10 μm), respectively. APS measures aerodynamic diameters, thus these are converted to geometric diameter by multiplying aerodynamic diameter by $\sqrt{X/\rho}$ (valid in the continuum regime that is where most of the coarse mode aerosol mass is in this study) assuming dynamic shape factor ($X = 1.6$) and density ($\rho = 2.6 \text{ g/cm}^3$) of dust aerosols, which we assume dominates the coarse mode aerosol. This assumption is based on the fact that AMS and SAGA measured similar concentrations of inorganic species (Figure 3a), and thus sulfate, ammonium, chloride and nitrate was mostly not present in sizes covered by SAGA but not by AMS. But since the aerosol size distribution measurements do show aerosol presence in these coarse sizes, we assume it is dominated by dust. Although LAS measures geometric diameter when particles are spherical, it is calibrated with NIST traceable polystyrene latex spheres (PSL), which have a larger refractive index (1.595) than the mixtures measured during the flight. Thus, LAS diameters are multiplied by 1.115 to approximately correct for this difference (Nault et al., 2018). While LAS and APS results are reported at 1 Hz frequency, SMPS provides data every minute. Since most datasets used in this work are provided at 1 Hz, we use nearest neighbor interpolation to assign SMPS values at 1 Hz resolution. This is likely to have negligible impact in our results as there is little aerosol mass in the bins assigned from the SMPS and mass extinction efficiency is low at these sizes. Previous studies have found a saturation of the LAS detector for large aerosol number and mass concentrations (Liu et al., 2017; Nault et al., 2018), which occurs when scattering from individual particles start overlapping so that the signal does not go down to the baseline between events. This was the case for a large fraction of the measurements in the haze layer during the flight studied. Figure 3b shows that while this saturation is evident for large aerosol mass concentrations, for lower aerosol mass concentrations (where no saturation is expected) the LAS measures larger volume concentrations than the AMS+SP2 by ~11%. Although 11% falls within the stated accuracies of both measurements, it is also potentially reflecting a true difference in concentrations. The AMS detected exotic metals not typically reported, such as rubidium (Figure 4a), in the haze event. There was, on average, 10 ng sm^{-3} rubidium in the plume between 01:30 to 05:00 UTC (and up to 71 ng sm^{-3}). Rubidium originates either from soil (e.g., dust) (Kabata-Pendias and Pendias, 2001) or anthropogenic emissions, such as dust from steel and aluminum industries (Dillner et al., 2006; Tang et al., 2018). Rubidium is one of numerous types of metal emitted from these sources and would account for the minority of the mass for these emissions (Dillner et al., 2006). Also, the detection shown here is likely a lower limit of the actual concentrations considering the refractory nature of the aerosols typically containing rubidium. The presence of rubidium would suggest other inorganic material present in the haze event not typically measured by the AMS, suggesting the 11% difference in volume is due to these types of compounds. Thus, we corrected the LAS submicron number and volume distributions using the aerosol mass measured by the AMS+SP2



235 accounting for the ~11% volume not detected. For this, scaling factors were computed using the aerosol volume (estimated
using the measured aerosol mass and the aerosol density reported by the AMS), corrected by 11%, and dividing by the
measured LAS volume, accounting for the AMS transmission. The AMS transmission considers 100% and 0% efficiency at
aerodynamic diameters of 550 nm and 1.5 μm , respectively, and a linear decrease in between using the logarithm of the
aerodynamic diameters (Hu et al., 2017). The transmission curve was converted to geometric diameter for each observation
240 using Equation 28 from DeCarlo et al. (2004) iteratively to update the Cunningham slip correction factor until convergence.
The LAS correction assumes that the fractional contribution of aerosol not measured by AMS+SP2 is constant, which is a
limitation of the approach, but we expect it to have limited impact in the analysis due to the small contribution. Submicron
dust aerosol mass concentration is estimated using this volume residual, assuming dust density of 2.6 g/cm^3 (value used in
WRF-Chem), and falls into the OIN aerosol category when comparing to model estimates.

245 **2.4. Ground based observations**

We also used multiple sources of ground-based observations. This includes Level 1.5 AOD at 500 nm wavelength, which
was obtained from the Aerosol Robotic Network (AERONET) version 3 algorithm (Giles et al., 2019; Eck et al., 2018).
During KORUS-AQ, the AERONET network in South Korea was enhanced by adding additional sites and thus a total of 21
locations were available during the campaign period (<https://aeronet.gsfc.nasa.gov/>). We also used $\text{PM}_{2.5}$ and PM_{10} from the
250 air quality network maintained by Korean National Institute of Environmental Research (NIER). For the period analyzed,
 $\text{PM}_{2.5}$ and PM_{10} data were available from 320 and 329 locations, respectively, distributed across the peninsula.

3. Results and discussion

3.1 Forecast evaluation

Figure 5a shows comparisons of AOD measured by the AERONET network over South Korea versus forecasted AOD at the
255 site locations. The model shows good performance over the period. This performance is expected as the system is
assimilating satellite AOD, and satellite AOD retrievals have shown good agreement with AERONET data in the region
(Choi et al., 2019b). However, the forecasts show large over-predictions of surface particulate matter for the period of large
concentrations in the peninsula, consistent with previously reported results (Lennartson et al., 2018). These over-predictions
are more severe for $\text{PM}_{2.5}$ during the passing of the transboundary pollution coming from China (May 24th and 25th),
260 sometimes exceeding a factor of two difference. This points towards model deficiencies in connecting surface mass
concentrations with column optical properties, which is explored in this study focusing on the day the aircraft sampled this
airmass (May 24th). Also, note that $\text{PM}_{2.5}$ and PM_{10} are similar in the model while PM_{10} is larger than $\text{PM}_{2.5}$ in the
observations, pointing towards model biases in representing coarse mode aerosols.

Figure 6 shows observed and forecasted AOD retrievals at noon local time the day of the May 24th DC-8 flight that sampled
265 the transboundary pollution that affected the Korean peninsula. The forecasts shown have not yet assimilated the AOD



retrieved that day, showing the ability of the system to carry forward the information assimilated the day before. AODs larger than 1 were found over areas in the Yellow Sea that were correctly forecasted and that enabled the KORUS-AQ team to plan a successful flight (track in yellow on the right panel of Figure 6) in the region. Data from this flight are used to perform a detailed model evaluation to understand the model biases.

270 One potential reason for the discrepancies found could be related to model representation of aerosol vertical profiles. Figure 7 shows aerosol extinction curtains over the DC-8 trajectory, as sampled by the DIAL-HSRL, and as predicted by the forecasts. The haze layer is mostly confined to below 2 km, which the model represents properly. The model has slightly higher mixing layers which, if anything, would lead to opposite biases (e.g., under-estimation of surface concentrations). A layer with lower aerosol extinction found between 2 and 6 km, which DIAL-HSRL classified as dust (not shown) and where
275 SAGA reported elevated levels of Ca^{+2} associated to dust, is also well captured by the model (in terms of both amount and aerosol type). Thus, we discard issues with model representation of the vertical placement of the plume as reasons for explaining the AOD to PM inconsistencies mentioned earlier.

AOD is also highly sensitive to relative humidity (Brock et al., 2016a) and previous studies have explained AOD biases due to model issues representing relative humidity (Feng et al., 2016). In-situ measurements of relative humidity in the haze
280 layer showed average values of 62% with an interquartile range of 9% (57-66 %). The forecast shows a reasonable representation with slightly higher average value (64%) and interquartile range (10%). Thus, we conclude skill in predicting relative humidity is not related to the discrepancies found in this study.

From this analysis, we conclude that the likely reason for the discrepancy resides in the computation of the aerosol optical properties, i.e., how aerosol mass is translated to AOD, and thus in the following sections we perform a thorough evaluation
285 of this topic using in-situ airborne data.

3.2 Closure studies

Model representation of optical properties can be separated into two stages: 1) how well the model represents the aerosol properties which drive the optical properties computation (e.g., size distribution, composition, concentrations, etc.); and, 2) the accuracy of the optical properties code. The latter can be evaluated by driving the optical properties code using observed
290 quantities and comparing the outputs with measurements of aerosol optical properties, a methodology that has been applied for previous field campaigns (Barnard et al., 2010; Brock et al., 2016a) and that we will refer to as “closure study” here. This allows us to isolate issues regarding the optical properties code and to assess ways to improve the model representation of optical properties.

One challenge of closure studies is that the optical properties code requires speciated and size-resolved aerosols, thus
295 assumptions need to be made on how to distribute the measured chemical species into the size bins. Figure 3a shows a scatter plots of SAGA filter-based vs AMS online measurements of inorganic aerosol mass concentrations (sulfate, nitrate, ammonium, chloride), showing good agreement for this flight. While secondary inorganic aerosol mass concentrations were elevated in the coarse mode for other KORUS-AQ flights (and thus not detected by AMS) (Heim et al., 2019), for the flight



analyzed here this fraction seems to be negligible. Thus, we assume that the tail of the coarse mode is composed of only OIN
300 (likely dust). We also assume that composition is not size dependent within the accumulation mode. Size resolved AMS
measurements support this assumption by showing similar composition within the accumulation mode (Fig 4b). We set the
aerosol diameter cut-off between the accumulation mode and the lower tail of the coarse mode at 884 nm, based on size
distribution measurements (Fig. 8). Also, since both LAS and APS cover the lower tail of the coarse mode we use APS
estimates in this range because LAS presents lower volume concentrations.

305 Figure 9 shows multiple statistical metrics in the form of box and whisker plots for observations and closure results during
the three consecutive hours that the DC-8 spent measuring the haze layer at multiple altitudes (2:00-5:00 UTC, see Figure 7).
The different closure scenarios are described in Table 4 and consist of the base configuration and then the base with varying
parameters such as the size bin resolution, refractive indices, and hygroscopicity parameter.

3.2.1 Dry extinction

310 A variable that is typically computed to assess the efficiency of an aerosol population at scattering light is the ratio between
dry scattering/extinction and aerosol mass concentrations, which is typically referred to as “mass scattering/extinction
efficiency”. Note that for this study, aerosol mass concentration corresponds to that measured by AMS+SP2. We also define
“volume extinction efficiency” as the ratio between dry extinction and aerosol volume concentration, obtained from the
aerosol size distribution measurements after performing the corrections described in section 2.3. As AMS and SP2 measure
315 mostly submicron aerosols of select chemical species, there is potential for unaccounted aerosol mass that is contributing to
aerosol extinction that could complicate the interpretation of the mass extinction efficiency. This is why the volume
extinction efficiency is reported in addition to the mass extinction efficiency as the extinction and volume are measured for
all aerosols in the same size range (behind the LARGE inlet).

Figure 9a,b clearly show how the base configuration of the optical properties code drastically under-predicts the dry
320 extinction produced by unit mass (and volume), consistent with the discrepancies shown in Figure 5. Aerosols are binned
into 4 size bins in the base configuration (Closure 1); thus, Closure 2 and 3 explore finer binning to 8 and 16 sections,
respectively. The finer binning does improve the performance, especially when going from 4 to 8 bins (Fig. 9a,b). Figure 8
shows the size distributions for the three types of size aggregation, showing a large diversity in the bin concentrations
contributing to the total mass in fine-resolution bins, which is lost when aggregating to coarser-resolution bins. Figure 10
325 shows steep changes in the volume extinction efficiency in the diameters where most of the aerosol mass is found. In the 4-
bin configuration, the whole accumulation mode is included in one bin. After aggregation, a mean diameter of 293 nm is
obtained, which has a volume extinction efficiency below $6 \text{ m}^2/\text{m}^3$ with base refractive indices. On the other hand, a large
percentage of the accumulation mode is found in bin #4 with the 8-bin configuration, which has a mean diameter of 380 nm
and a volume extinction efficiency of $\sim 8 \text{ m}^2/\text{m}^3$, which raises the overall efficiency substantially. The improvements from 8
330 to 16 bins are lower than from 4 to 8 bins, but still significant, and are due to similar reasons. For instance, bin #8 in the 16-



bin configuration shows volume extinction efficiency above $9 \text{ m}^2/\text{m}^3$, getting close to the maximum values for base refractive indices. Negligible improvements are found when further refining from 16 to 32 size bins (not shown). Although improvements are found when refining the size bins, significant biases still persist for the 16 bin configuration (Fig. 9a,b). Thus, we explore modifying the refractive indices used in the Mie calculation (see section 2.3), based on values reported in the literature for the aerosol species accounting for most submicron mass. Typical real refractive indices assumed in closure studies (e.g., Brock et al., 2016a) for ammonium-sulfate and ammonium-nitrate are 1.527 (Hand and Kreidenweis, 2002) and 1.553 (Tang, 1996) which are larger than those used in the base configuration, thus we update them accordingly. For primary and secondary organic aerosols, there is a large range of values found in the literature (e.g., Moise et al., 2015; Lu et al., 2015). Aldhaif et al. (2018) derived OA real refractive index from field deployments by air mass type, finding a mean value of 1.54 with 1.52-1.55 as the 25-75th percentile range for urban air masses. We chose the value of 1.55 as it is in the 25-75th percentile range and because it is a typical value used in past studies (Zhang et al., 1994; Hand and Kreidenweis, 2002; Hodzic et al., 2004). This value also corresponds to the mean real refractive index reported by Lu et al. (2015) for primary organic aerosol based on a literature review. The Closure 4 case includes these updates (summary of updated parameters in Table 2) showing an increase in the efficiencies which improves the model representation (Figure 9a,b). Although the mass and volume extinction efficiencies are still under-predicted, there is much better agreement when using the updated refractive indices, obtaining an overlap of the observed and modeled 25-75th percentile boxes. Besides the overall increase in the efficiencies, there is also a slight shift towards smaller sizes of the location where the efficiencies vs particle dry-diameter curve achieves its maximum (Figure 10a). The update in the OA refractive index generates the most impact (not shown) due to the larger increase (7% change vs 0.5% and 3.5% for ammonium sulfate and ammonium nitrate, respectively) and large contribution to the total mass (23% on average).

3.2.2 Hygroscopic growth

While the analysis in the previous sub-section was performed for the dry aerosol extinction, we also explored possible biases due to hygroscopic growth, considering that relative humidity was in the 50-80% range in the haze layer. We assessed the performance of the optical properties code, driven by observed inputs in representing the aerosol light scattering enhancement factor ($f(\text{RH})$), defined here as the ratio between 550 nm aerosol scattering at 80% (wet) and 20% (dry) relative humidity.

Figure 9c shows that the base configuration performs well for $f(\text{RH})$. This is due to a combination of the wrong reasons (i.e., cancellation of errors), as it deteriorates when increasing the size bin resolution (Closure 2 and 3) and upon increasing the refractive indices (Closure 4). Figure 10a additionally shows $f(\text{RH})$ and can help explain this behavior, as $f(\text{RH})$ has a strong decreasing trend with increasing diameter in the region $<350 \text{ nm}$. Thus, because the 4-bin representation displays an apparent decrease in the mean diameter (Figure 7), $f(\text{RH})$ is over-estimated. As the size bins are refined, less aerosol mass falls in the smaller size bins, decreasing the total $f(\text{RH})$. The further decrease of $f(\text{RH})$ with increasing refractive indices at these size ranges is also shown in Figure 10a. While our alternative approach at computing aerosol water uptake resulted in



values ~10% lower than that shown by WRF-Chem, the difference in the observed vs Closure4 $f(\text{RH})$ are close to 30%, thus
365 we conclude that similar biases would be expected for the WRF-Chem routines.

To improve the optical properties code performance, we updated the hygroscopicity parameter based on values found in the
literature for the species contributing to most of the aerosol mass. κ values are generally reported with large range of
uncertainty and can depend on the measurement technique and environmental conditions. Petters and Kreidenweis (2007)
show a wide range of κ values for ammonium sulfate, from 0.33 to 0.72 and a mean of 0.53, for κ derived using growth
370 factors, and a mean value of 0.61 based on CCN measurements. For ammonium nitrate, only CCN derived κ is available
with a mean value of 0.67 and a range of 0.577-0.753. We chose to use the mean values of the CCN-derived estimates (0.61
for ammonium sulfate and 0.67 for ammonium nitrate), as they are contained in the ranges provided in Petters and
Kreidenweis (2007) and in other studies (e.g., Good et al., 2010). For organic aerosol, the range is even larger. We chose to
treat organic aerosol and OIN as slightly hygroscopic, as it was originally specified in WRF-Chem parametrization for
375 GOCART, with κ values of 0.14 for both, which is consistent with values reported for aged urban OA and for rural
environments (Wang et al., 2010; Mei et al., 2013; Levin et al., 2014). A summary of the updated κ values can be found on
Table 2. Figure 9c shows significant increases in $f(\text{RH})$ from Closure 4 to Closure 5, as expected, from the increases in the
hygroscopicity parameter up to a similar level as the observations. Sensitivity analysis shows that most of the change is
related to the κ increases in ammonium sulfate and ammonium nitrate due to their larger contribution to mass fraction (62%
380 on average), while additional water uptake of organics and other inorganic aerosols play a minor role. Thus, choosing a
lower OA κ value more consistent with other studies (Brock et al., 2016a; Shingler et al., 2016) would have resulted in
similar findings.

3.2.3 Other aerosol optical properties

Figures 9d and 9e show the change for the Angstrom Exponent (AE) and single-scattering albedo (SSA) for the different
385 model closure configurations shown. Overall, the representation of both AE and SSA improve when going from the coarse
size bin resolution and base parameters to the finer bin and updated parameters, which represents independent pieces of
evidence that the change in configuration is in the right direction. As seen in Figure 10b, AE is sensitive to the aerosol size
distribution and generally decreases with larger aerosol sizes. This explains the sharp decrease when refining the aerosol size
bins (Closure 1 to Closure 2), due to the lower mean diameters for the 4-bin configuration as described previously. Figure 9e
390 shows that SSA gradually increases with the change of configuration, which is due to changes in mean diameters and higher
scattering when increasing the real refractive indices (Fig 10b). While the AE of Closure 5 matches very well with the
observed values (mostly due to improvements from Closure 1 to 2), SSA is still slightly under-predicted, which is an issue
previously identified in other closure studies using a similar approach for computing aerosol optical properties (Barnard et
al., 2010). This under-estimation could be due to multiple uncertainties including assumptions on black carbon and OIN
395 complex refractive indices, black carbon mixing state, and size-independent black carbon fractional contribution to the
accumulation mode.



3.3 Evaluation of retrospective simulations

The previous section provides clarity on what we should expect from the optical properties code if the model was reproducing observed aerosol size distributions and composition. In this section we perform a similar analysis but driving the optical properties code with simulated aerosol properties (summarized in Table 1 and shown in Figure 11). Comparing Figures 11a and 11b, we can see large discrepancies in the performance of the mass and volume extinction efficiencies, opposite to the closure studies (Figure 9) where they remain consistent. For instance, MOSAIC4b shows good representation for the mass extinction efficiency against Closure 5 but largely under-estimates the volume extinction efficiency. Comparing Figure 11 and 9, the mass extinction efficiency is shifted up in the three base modeling configurations, and thus a refinement in size bins (going from MOSAIC4bin to MOSAIC8b or RACM1) has the opposite effect on performance for mass and volume extinction efficiencies. The modeled aerosol mass concentration used when computing the mass extinction efficiency is that for which the AMS transmission is applied. Thus, one possible explanation could be that the models have significant aerosol mass outside of the sizes where the AMS can detect. This would reduce the mass concentration after applying the transmission curve which would increase the extinction to mass ratio (i.e., the mass extinction efficiency) due to the unaccounted mass that contributes to extinction. Figure 12 shows the size distributions for the simulations, where this issue is evident as all three base model configurations (MOSAIC4b, MOSAIC8b and RACM1) place substantial aerosol accumulation mode mass in sizes where the AMS transmission starts decreasing (> 625 nm). This is not the case for the observed size distribution (Fig. 8), where most accumulation mode aerosol mass is within the AMS transmission and explains the consistency between mass and volume extinction efficiency for closure studies.

Another contributor to this discrepancy is the model prediction of chemical composition. Figure 13 shows that, although OIN absolute concentrations are in the range of the observations, all modeling configurations over-predict the fractional contribution of submicron OIN mass (17-28% vs 12% in the observations), with the MOSAIC configurations showing larger over-predictions. Since the aerosol mass used in the mass extinction efficiency corresponds to that measured by AMS+SP2 where OIN is not included, then over-predicting the OIN fraction would increase the mass not accounted for in the ratio, increasing it relative to the observations. Potential reasons contributing to the over-prediction in OIN fraction include: (1) an over-prediction of the “other PM_{2.5}” anthropogenic emission category and/or distributing it in the accumulation mode as opposed to in the lower tail of the coarse mode; (2) over-prediction of fine mode by wind-blown dust parameterizations (Kok, 2011); and/or, (3) insufficient production of secondary organic and inorganic aerosols (see under-prediction on left panel of Fig. 13), which has the effect of increasing the fractional contribution of the primary aerosol species (OIN in this case). Under-predictions of organic aerosol could be explained by large variations of secondary organic aerosol production within urban areas (Nault et al., 2018) that are not captured by the modeling configurations. Under-predictions of secondary inorganics could be due to missing mechanisms to produce sulfate during Chinese haze conditions (e.g., Gao et al., 2016a). These mechanisms were not included in this study as uncertainties remain on the actual pathways (Guo et al., 2017) and representation in models (Song et al., 2018). Other potential reasons for the under-estimate on secondary inorganics could



430 include slow in-cloud H_2O_2 oxidation of SO_2 due to under-estimates of cloud volume and NO_x underpredictions (e.g., Goldberg et al., 2019b).

Another point to note is that models under-predict the relative magnitude of the coarse aerosols (2.5-10 μm range, bin #4 in the 4-bin configuration). This helps to explain why the biases shown in Figure 5 are more pronounced for $\text{PM}_{2.5}$ than PM_{10} , as the under-prediction in the coarse aerosols is offset by the over-prediction in the fine aerosols.

435 As mentioned earlier, all three base modeling configurations have issues representing the size distribution regardless of the large diversity in chemical and aerosol scheme. This is a topic that needs to be explored further in a future dedicated study. In the case of the MOSAIC configurations, the shape of the size distribution evolves through aerosol processes (coagulation, condensation, etc.). Since these processes that modify the size distribution are reasonably well known (Seinfeld and Pandis, 2016), it is unlikely such large errors would arise from the model implementation of these processes. A more likely
440 explanation is that the shape of the size distribution established at the point of emission is too wide to start with and unfolds into the results shown. In the case of the RACM1 configuration, the widths of the log-normal modes are controlled by the geometric standard deviation (GSD). In the WRF-Chem implementation the GSD is fixed at 1.7, 2.0, and 2.5 for nuclei, accumulation and coarse modes, respectively. Changing the GSD to 1.6 for both the nuclei and accumulation mode (i.e., RACM2 simulations) results in a better representation of the observed aerosol size distribution (Fig. 12 vs Fig. 8), with a
445 narrower accumulation mode peaking in the 300-450 nm range and much smaller mass contribution in sizes above 625 nm. These results are consistent with Brock et al. (2016b), which showed that GSD in the southeastern US are in the 1.4-1.6 range while chemistry-climate models generally over-predict it by using a GSD value of 2.0.

After correcting the modeled size distribution, a larger percentage of the aerosol mass is found within the AMS transmission (see increase in mass for all species from RACM1 to RACM2 in left panel of Fig. 13). Also, the model representation of
450 mass and volume extinction efficiency against observations now follows the same trend for RACM2 (Figure 11a,b) but minor discrepancies still remain (e.g., mass extinction efficiency performs well against Closure 5 but volume extinction efficiency slightly under-predicts). Besides the over-prediction of the OIN fraction mentioned earlier, the remaining discrepancy can also be explained by the aerosol density used for organic aerosols (OA) in the model. For the closure study, OA mass is converted to volume using the density reported by the AMS, which varies substantially with the oxidation state
455 of organic aerosol (Kuwata et al., 2012). For the period analyzed here, the OA density has a mean of 1.5 g/cm^3 and 25th and 75th percentiles of 1.35 g/cm^3 and 1.6 g/cm^3 , respectively. In the case of the simulations, the aerosol optical properties code in WRF-Chem uses a constant OA density of 1.0 g/cm^3 . Thus, a lower density translates into larger volume per unit mass, increasing the mass extinction efficiency and explaining the remaining discrepancy. On the other hand, volume extinction efficiency is less sensitive to changes in aerosol density as a decrease in density decreases both extinction and volume. In
460 fact, the volume extinction efficiency remains consistent with the analyses shown in the previous section when changing size distribution and aerosol density. Thus, we use volume extinction efficiency in the following analysis.

As shown in Figure 11b, the dry extinction to volume ratio is greatly under-estimated by almost a factor of two by the MOSAIC4b simulation, which helps explain the discrepancy described in Figure 5. As described in the previous section,



large improvements are found when computing optical properties using finer aerosol bin representation (MOSAIC8b and
465 RACM1) with some remaining biases. This large improvement from the 4 to 8 bin configuration is in agreement with
previous studies that found an overall consistency between AOD and surface PM when using 8 size bins (Saide et al., 2014;
Gao et al., 2016b; Gao et al., 2015). Surprisingly, simulations with better aerosol size distribution representation (RACM2)
do not significantly modify the representation of the volume and mass extinction efficiency. Figures 12 and 10 show that
both size distributions (RACM1 and RACM2 for the 8-bin configuration) are centered in a size range with high mass
470 extinction efficiency ($\sim 9 \text{ m}^2/\text{g}$ around 400 nm diameter). While the original size distribution has less mass assigned to this
high efficiency bin, it has substantial mass in larger size ranges where mass extinction efficiency is still high ($\sim 7 \text{ m}^2/\text{g}$ at
 $\sim 800 \text{ nm}$ diameter). On the other hand, the updated size distribution has larger mass in smaller size bins where mass
extinction efficiency drops substantially ($\sim 3\text{-}4 \text{ m}^2/\text{g}$ at 200-250 nm diameter). Thus, the overall mass extinction efficiency
remains similar for both size distribution due to compensating effects. As performed in the previous section, a sensitivity
475 simulation is carried out such that the refractive indices of selected species are increased (RACM3,4), which bring the ratios
to similar levels as the Closure 5 (Figure 11b).

In terms of aerosol hygroscopic growth and its effects on scattering, all base simulations under-predict $f(\text{RH})$, which also
helps explain the discrepancies shown in Figure 5. Improving the size distribution (RACM2) has a small but positive effect
on $f(\text{RH})$ representation. The largest improvement is found when updating the hygroscopicity parameters for the same
480 species updated in Closure 5 (RACM4). After this, a slight under-prediction is still found. A possible contribution to this bias
could be linked to the simulations not representing the aerosol chemical composition properly. As seen in Figure 13,
RACM2 reasonably represents the observed pie-chart but does show a slight over-prediction of the less hydrophilic species
(sum of OA, BC and OIN is 44% vs 37% in the observations). Another contributor to this bias is the low OA density used in
the retrospective simulations. Using a lower aerosol density has a similar effect as using larger refractive index (more
485 extinction per unit mass) and, as seen in Figure 10a, increasing the refractive index reduces $f(\text{RH})$ explaining the bias.
Sensitivity analysis using observed OA density confirms this finding (not shown).

AE performance improves drastically when the size resolution is improved (RACM1 to RACM2) as the size distribution is
shifted to smaller sizes, increasing AE. The AE after all the updates (RACM4) is still low, which is partially related to the
low OA density but also might be associated with the size distribution. Out of the base simulations, SSA performance is
490 better for the RACM1 simulation as MOSAIC8b over-predicts the black carbon fraction and MOSAIC4b has a coarse size
bin representation (see previous section). After the updates (RACM4), SSA skill is comparable to that of the Closure 5 study
likely due to BC being well represented both in magnitude and fractional contribution (RACM2 results shown in Figure 13
are similar to those from RACM4).



4. Conclusions

495 In this study, we first evaluated WRF-Chem forecasts, which included assimilation of AOD, performed to support flight
planning during the NASA/NIER KORUS-AQ field campaign. While forecasts showed accurate predictions of aerosol
optical depth, there were over-predictions of surface particulate matter in the Korean peninsula, with the largest deviations
occurring for PM_{2.5} during a transboundary pollution event. Additional analysis showed that the model was able to capture
the vertical extent and the relative humidity of the haze layer, pointing towards issues related to the aerosol mass to optical
500 properties calculation.

Further analysis was split in two sections. First, a closure study was performed by driving the optical properties
parametrization with in-situ observations of aerosol size distributions and composition collected by the DC-8 aircraft. These
were compared to measured optical properties, including mass and volume extinction efficiencies, hygroscopic growth
represented by $f(\text{RH})$, Angstrom Exponent, and single-scattering albedo (SSA). This analysis showed closure was not
505 possible by the base configuration and that multiple modifications were needed to achieve closure. These included driving
the optical properties code with finer size bin representation (from 4 up to 16 bins), increasing refractive indices of
ammonium nitrate (to 1.553) and organic aerosol (to 1.55) according to ranges found in the recent literature, and increasing
hygroscopicity parameter of ammonium sulfate (to 0.61), ammonium nitrate (to 0.67), organic aerosol (to 0.14), and other
inorganics (to 0.14) within published ranges. The coarse bin representation and low values of refractive indices and
510 hygroscopicity parameters explain why the forecasts showed the largest discrepancies during the haze event, as these events
are associated with large relative humidity and aerosol size distributions that peak close to the maximum mass extinction
efficiencies.

Second, aerosol optical and microphysical properties were evaluated for retrospective simulations using three different
aerosol models within WRF-Chem. This exercise additionally found that all three aerosol models were unable to properly
515 capture the aerosol size distribution, showing a larger size range than what was observed. As a result, a substantial fraction
of modeled aerosol mass was in sizes where the AMS transmission starts decreasing, which led to discrepancies between the
modeled mass and volume extinction efficiencies. We also found that, while the model uses a value of 1.0 g/cm³ for organic
aerosol density, larger values were observed with a mean of ~1.5 g/cm³ and considerable variability, which generated further
discrepancies and reduced the skill in predicting some of the optical properties. Other issues included an over-prediction of
520 the OIN fractional contribution by all models (which could be due to issues with OIN emissions and/or secondary aerosol
formation). The size distribution of a configuration using a modal scheme improved by reducing the geometric standard
deviation (GSD) of the accumulation mode from 2.0 to 1.6. Further increasing the refractive indices and hygroscopicity
parameters (as noted above) provided overall better representation of optical properties. Future work needs to assess if the
simulated size distributions can be improved by including primary aerosol emissions in the model using size-resolved and
525 source-specific observational datasets (Winijkul et al., 2015; Lu et al., 2015).



A series of assumptions were made in this study that should be considered when analyzing the results. One of them corresponds to the correction of the LAS measurements to account for the PSL calibration and for the saturation of the instrument at high aerosol concentrations. The calibration correction was performed by applying a single scaling factor to the measured diameters which may not be constant due to changes in aerosol size and composition (Kupc et al., 2018). In addition, the saturation correction was applied for all LAS size bins equally, while the saturation of the instrument is both a function of particle concentration and size. The use of these assumptions could impact the results which could account for some of the minor mismatches found between observations and the Closure study after accounting for possible model uncertainties (Closure 5). The LAS was the only instrument on board sampling the overall aerosol size distribution over the ranges where the accumulation mode peaked, so it would be useful for future field campaigns to have overlapping instruments with similar capabilities over this size range or dilute the sample during high concentration events as has been done in other deployments (Brock et al., 2019).

Consistency of relationships between AOD and PM in models is a key element in effectively improving predictions through data assimilation of AOD and/or PM mass. This work found that multiple sources of model uncertainties need to be addressed to provide accurate representation of optical properties and avoid mismatches when performing data assimilation driven by AOD observations. These include the use of fine aerosol size representation in optical properties calculations and improved representation of aerosol properties (size distribution, chemical composition, refractive index, hygroscopicity parameter, density). Accurate representation of aerosol optical properties is also important for other fields that use these models to make the connection between aerosol mass concentrations and aerosol optical properties, including assessments of aerosol health effects based on satellite data, proper projections of aerosol-radiation interactions done by climate models, visibility forecasts, and solar power predictions for energy applications.

In this study we evaluated different configuration of the WRF-Chem model for the specific case of anthropogenic outflow from China, thus future studies can perform similar analysis for other types of air masses and assess if the model configuration updates suggested here produce better results in other scenarios. Also, similar analysis is also needed for other air quality and chemistry-climate models to assess if similar biases or different ones arise.

550 **Code and data availability**

The WRF-Chem code and satellite AOD retrievals used in this study is available upon request. Korean air quality data can be found in <http://www.airkorea.or.kr>, AERONET data is available at <https://aeronet.gsfc.nasa.gov/>, and KORUS-AQ data and flight reports are public at <https://www-air.larc.nasa.gov/missions/korus-aq/>. Contact P.E. Saide (saide@atmos.ucla.edu) for data requests.



555 Author contributions

PES designed and executed the study and led the writing of the manuscript. AB, CAC, KLT, BA, JWH, ARN, GSD, JLJ, BAN, PCJ, JD, EH, KL. JPS, SEP, JK, MC, and BH provided observational data. GP and AH provided code. All co-authors contributed with feedback during the development and writing of the study.

Competing interests

560 The authors declare that they have no conflict of interest.

Acknowledgments

We thank all KORUS-AQ participants that made the field experiment possible. We also thank the PIs and their staff of all the AERONET sites in South Korea for establishing and maintaining them. This work was carried out with the aid of NASA grants NNX11AI52G, NNX16AD96G, NNX15AT96G, NNX15AT88G, NNH15AB60I, and 80NSSC19K0124. Its contents
565 are solely the responsibility of the authors and do not necessarily represent the official views of the funding institutions. The National Center for Atmospheric Research is sponsored by the National Science Foundation.

References

- Ahmadov, R., McKeen, S. A., Robinson, A. L., Bahreini, R., Middlebrook, A. M., de Gouw, J. A., Meagher, J., Hsie, E.-Y., Edgerton, E., Shaw, S., and Trainer, M.: A volatility basis set model for summertime secondary organic aerosols over the
570 eastern United States in 2006, *Journal of Geophysical Research: Atmospheres*, 117, 10.1029/2011jd016831, 2012.
- Ahmadov, R., McKeen, S., Trainer, M., Banta, R., Brewer, A., Brown, S., Edwards, P. M., de Gouw, J. A., Frost, G. J., Gilman, J., Helmig, D., Johnson, B., Karion, A., Koss, A., Langford, A., Lerner, B., Olson, J., Oltmans, S., Peischl, J., Pétron, G., Pichugina, Y., Roberts, J. M., Ryerson, T., Schnell, R., Senff, C., Sweeney, C., Thompson, C., Veres, P., Warneke, C., Wild, R., Williams, E. J., Yuan, B., and Zamora, R.: Understanding high wintertime ozone pollution events in
575 an oil and natural gas producing region of the western US, *Atmos. Chem. Phys. Discuss.*, 14, 20295-20343, 10.5194/acpd-14-20295-2014, 2014.
- Aknan, A., and Chen, G.: KORUS-AQ DC-8 Aircraft Dataset, [online] Available from: <https://www-air.larc.nasa.gov/cgi-bin/ArcView/korusaq> (Accessed 6 February 2019), 10.5067/Suborbital/KORUSAQ/DATA01. 2019.
- Aldhaif, A. M., Stahl, C., Braun, R. A., Moghaddam, M. A., Shingler, T., Crosbie, E., Sawamura, P., Dadashazar, H.,
580 Ziemba, L., Jimenez, J. L., Campuzano-Jost, P., and Sorooshian, A.: Characterization of the Real Part of Dry Aerosol Refractive Index Over North America From the Surface to 12 km, *Journal of Geophysical Research: Atmospheres*, 123, 8283-8300, 10.1029/2018jd028504, 2018.



- Barnard, J. C., Fast, J. D., Paredes-Miranda, G., Arnott, W. P., and Laskin, A.: Technical Note: Evaluation of the WRF-Chem "Aerosol Chemical to Aerosol Optical Properties" Module using data from the MILAGRO campaign, *Atmos. Chem. Phys.*, 10, 7325-7340, 10.5194/acp-10-7325-2010, 2010.
- 585
- Benedetti, A., Morcrette, J., Boucher, O., Dethof, A., Engelen, R., Fisher, M., Flentje, H., Huneeus, N., Jones, L., and Kaiser, J.: Aerosol analysis and forecast in the European Centre for Medium-Range Weather Forecasts Integrated Forecast System: 2. Data assimilation, *J. Geophys. Res.*, 114, D13205, 2009.
- Bohren, C. F., and Huffman, D. R.: *Absorption and scattering of light by small particles*, Wiley, New York, 1983.
- 590
- Boucher, O., Randall, D., Artaxo, P., Bretherton, C., Feingold, G., Forster, P., Kerminen, V.-M., Kondo, Y., Liao, H., Lohmann, U., Rasch, P., Satheesh, S. K., Sherwood, S., Stevens, B., and Zhang, X. Y.: *Clouds and Aerosols*. In: *Climate Change 2013: The Physical Science Basis. Contribution of Working Group I to the Fifth Assessment Report of the Intergovernmental 25 Panel on Climate Change*, edited by: Stocker, T. F., Qin, D., Plattner, G.-K., Tignor, M., Allen, S. K., Boschung, J., Nauels, A., Xia, Y., Bex, V., and Midgley, P. M, Cambridge University Press, Cambridge, United Kingdom
- 595
- and New York, NY, USA, 2013.
- Brock, C. A., Wagner, N. L., Anderson, B. E., Attwood, A. R., Beyersdorf, A., Campuzano-Jost, P., Carlton, A. G., Day, D. A., Diskin, G. S., Gordon, T. D., Jimenez, J. L., Lack, D. A., Liao, J., Markovic, M. Z., Middlebrook, A. M., Ng, N. L., Perring, A. E., Richardson, M. S., Schwarz, J. P., Washenfelder, R. A., Welti, A., Xu, L., Ziemba, L. D., and Murphy, D. M.: Aerosol optical properties in the southeastern United States in summer – Part 1: Hygroscopic growth, *Atmos. Chem. Phys.*, 16, 4987-5007, 2016a.
- 600
- Brock, C. A., Wagner, N. L., Anderson, B. E., Beyersdorf, A., Campuzano-Jost, P., Day, D. A., Diskin, G. S., Gordon, T. D., Jimenez, J. L., Lack, D. A., Liao, J., Markovic, M. Z., Middlebrook, A. M., Perring, A. E., Richardson, M. S., Schwarz, J. P., Welti, A., Ziemba, L. D., and Murphy, D. M.: Aerosol optical properties in the southeastern United States in summer – Part 2: Sensitivity of aerosol optical depth to relative humidity and aerosol parameters, *Atmos. Chem. Phys.*, 16, 5009-5019, 10.5194/acp-16-5009-2016, 2016b.
- 605
- Brock, C. A., Williamson, C., Kupc, A., Froyd, K. D., Erdesz, F., Wagner, N., Richardson, M., Schwarz, J. P., Gao, R. S., Katich, J. M., Campuzano-Jost, P., Nault, B. A., Schroder, J. C., Jimenez, J. L., Weinzierl, B., Dollner, M., Bui, T., and Murphy, D. M.: Aerosol size distributions during the Atmospheric Tomography Mission (ATom): methods, uncertainties, and data products, *Atmos. Meas. Tech.*, 12, 3081-3099, 10.5194/amt-12-3081-2019, 2019.
- Chin, M., Ginoux, P., Kinne, S., Torres, O., Holben, B. N., Duncan, B. N., Martin, R. V., Logan, J. A., Higurashi, A., and
- 610
- Nakajima, T.: Tropospheric Aerosol Optical Thickness from the GOCART Model and Comparisons with Satellite and Sun Photometer Measurements, *Journal of the atmospheric sciences*, 59, 461-483, 10.1175/1520-0469(2002)059<0461:taotft>2.0.co;2, 2002.
- Choi, J., Park, R. J., Lee, H.-M., Lee, S., Jo, D. S., Jeong, J. I., Henze, D. K., Woo, J.-H., Ban, S.-J., Lee, M.-D., Lim, C.-S., Park, M.-K., Shin, H. J., Cho, S., Peterson, D., and Song, C.-K.: Impacts of local vs. trans-boundary emissions from different
- 615
- sectors on PM_{2.5} exposure in South Korea during the KORUS-AQ campaign, *Atmospheric Environment*, 203, 196-205, <https://doi.org/10.1016/j.atmosenv.2019.02.008>, 2019a.



- Choi, M., Kim, J., Lee, J., Kim, M., Park, Y. J., Jeong, U., Kim, W., Hong, H., Holben, B., Eck, T. F., Song, C. H., Lim, J. H., and Song, C. K.: GOCI Yonsei Aerosol Retrieval (YAER) algorithm and validation during the DRAGON-NE Asia 2012 campaign, *Atmos. Meas. Tech.*, 9, 1377-1398, 10.5194/amt-9-1377-2016, 2016.
- 620 Choi, M., Kim, J., Lee, J., Kim, M., Park, Y. J., Holben, B., Eck, T. F., Li, Z., and Song, C. H.: GOCI Yonsei aerosol retrieval version 2 products: an improved algorithm and error analysis with uncertainty estimation from 5-year validation over East Asia, *Atmos. Meas. Tech.*, 11, 385-408, 10.5194/amt-11-385-2018, 2018.
- Choi, M., Lim, H., Kim, J., Lee, S., Eck, T. F., Holben, B. N., Garay, M. J., Hyer, E. J., Saide, P. E., and Liu, H.: Validation, comparison, and integration of GOCI, AHI, MODIS, MISR, and VIIRS aerosol optical depth over East Asia during the 2016
- 625 KORUS-AQ campaign, *Atmos. Meas. Tech.*, 12, 4619-4641, 10.5194/amt-12-4619-2019, 2019b.
- Clark, P. A., Harcourt, S. A., Macpherson, B., Mathison, C. T., Cusack, S., and Naylor, M.: Prediction of visibility and aerosol within the operational Met Office Unified Model. I: Model formulation and variational assimilation, *Quarterly Journal of the Royal Meteorological Society*, 134, 1801-1816, 10.1002/qj.318, 2008.
- Cohen, A. J., Brauer, M., Burnett, R., Anderson, H. R., Frostad, J., Estep, K., Balakrishnan, K., Brunekreef, B., Dandona, L.,
- 630 Dandona, R., Feigin, V., Freedman, G., Hubbell, B., Jobling, A., Kan, H., Knibbs, L., Liu, Y., Martin, R., Morawska, L., Pope, C. A., III, Shin, H., Straif, K., Shaddick, G., Thomas, M., van Dingenen, R., van Donkelaar, A., Vos, T., Murray, C. J. L., and Forouzanfar, M. H.: Estimates and 25-year trends of the global burden of disease attributable to ambient air pollution: an analysis of data from the Global Burden of Diseases Study 2015, *The Lancet*, 389, 1907-1918, 10.1016/S0140-6736(17)30505-6, 2017.
- 635 Crippa, P., Sullivan, R. C., Thota, A., and Pryor, S. C.: Sensitivity of Simulated Aerosol Properties Over Eastern North America to WRF-Chem Parameterizations, *Journal of Geophysical Research: Atmospheres*, 124, 3365-3383, 10.1029/2018JD029900, 2019.
- DeCarlo, P. F., Slowik, J. G., Worsnop, D. R., Davidovits, P., and Jimenez, J. L.: Particle Morphology and Density Characterization by Combined Mobility and Aerodynamic Diameter Measurements. Part 1: Theory, *Aerosol Science and*
- 640 *Technology*, 38, 1185-1205, 10.1080/027868290903907, 2004.
- DeCarlo, P. F., Kimmel, J. R., Trimborn, A., Northway, M. J., Jayne, J. T., Aiken, A. C., Gonin, M., Fuhrer, K., Horvath, T., Docherty, K. S., Worsnop, D. R., and Jimenez, J. L.: Field-Deployable, High-Resolution, Time-of-Flight Aerosol Mass Spectrometer, *Analytical Chemistry*, 78, 8281-8289, 10.1021/ac061249n, 2006.
- Dibb, J. E., Talbot, R. W., and Scheuer, E. M.: Composition and distribution of aerosols over the North Atlantic during the
- 645 Subsonic Assessment Ozone and Nitrogen Oxide Experiment (SONEX), *Journal of Geophysical Research: Atmospheres*, 105, 3709-3717, 2000.
- Dillner, A. M., Schauer, J. J., Zhang, Y., Zeng, L., and Cass, G. R.: Size-resolved particulate matter composition in Beijing during pollution and dust events, *Journal of Geophysical Research: Atmospheres*, 111, 10.1029/2005jd006400, 2006.
- Eck, T. F., Holben, B. N., Reid, J. S., Xian, P., Giles, D. M., Sinyuk, A., Smirnov, A., Schafer, J. S., Slutsker, I., Kim, J.,
- 650 Koo, J.-H., Choi, M., Kim, K. C., Sano, I., Arola, A., Sayer, A. M., Levy, R. C., Munchak, L. A., O'Neill, N. T., Lyapustin,



- A., Hsu, N. C., Randles, C. A., Da Silva, A. M., Buchard, V., Govindaraju, R. C., Hyer, E., Crawford, J. H., Wang, P., and Xia, X.: Observations of the Interaction and Transport of Fine Mode Aerosols With Cloud and/or Fog in Northeast Asia From Aerosol Robotic Network and Satellite Remote Sensing, *Journal of Geophysical Research: Atmospheres*, 123, 5560-5587, 10.1029/2018jd028313, 2018.
- 655 Fast, J. D., Gustafson Jr, W. I., Easter, R. C., Zaveri, R. A., Barnard, J. C., Chapman, E. G., Grell, G. A., and Peckham, S. E.: Evolution of ozone, particulates, and aerosol direct radiative forcing in the vicinity of Houston using a fully coupled meteorology-chemistry-aerosol model, *Journal of Geophysical Research*, 111, D21305, 2006.
- Feng, Y., Cadetdu, M., Kotamarthi, V. R., Renju, R., and Suresh Raju, C.: Humidity Bias and Effect on Simulated Aerosol Optical Properties during the Ganges Valley Experiment, *Current Science (Bangalore)*, Medium: X; Size: Article No. 93; 660 100, 2016.
- Gakidou, E., et al.: Global, regional, and national comparative risk assessment of 84 behavioural, environmental and occupational, and metabolic risks or clusters of risks, 1990-2016: a systematic analysis for the Global Burden of Disease Study 2016, *The Lancet*, 390, 1345-1422, 10.1016/S0140-6736(17)32366-8, 2017.
- Gao, M., Carmichael, G. R., Wang, Y., Ji, D., Liu, Z., and Wang, Z.: Improving simulations of sulfate aerosols during winter 665 haze over Northern China: the impacts of heterogeneous oxidation by NO₂, *Frontiers of Environmental Science & Engineering*, 10, 16, 2016a.
- Gao, M., Carmichael, G. R., Wang, Y., Saide, P. E., Yu, M., Xin, J., Liu, Z., and Wang, Z.: Modeling study of the 2010 regional haze event in the North China Plain, *Atmos. Chem. Phys.*, 16, 1673-1691, 10.5194/acp-16-1673-2016, 2016b.
- Gao, Y., Zhang, M., Liu, Z., Wang, L., Wang, P., Xia, X., Tao, M., and Zhu, L.: Modeling the feedback between aerosol and 670 meteorological variables in the atmospheric boundary layer during a severe fog-haze event over the North China Plain, *Atmos. Chem. Phys.*, 15, 4279-4295, 10.5194/acp-15-4279-2015, 2015.
- Giles, D. M., Sinyuk, A., Sorokin, M. G., Schafer, J. S., Smirnov, A., Slutsker, I., Eck, T. F., Holben, B. N., Lewis, J. R., Campbell, J. R., Welton, E. J., Korkin, S. V., and Lyapustin, A. I.: Advancements in the Aerosol Robotic Network (AERONET) Version 3 database – automated near-real-time quality control algorithm with improved cloud 675 screening for Sun photometer aerosol optical depth (AOD) measurements, *Atmos. Meas. Tech.*, 12, 169-209, 10.5194/amt-12-169-2019, 2019.
- Goldberg, D. L., Gupta, P., Wang, K., Jena, C., Zhang, Y., Lu, Z., and Streets, D. G.: Using gap-filled MAIAC AOD and WRF-Chem to estimate daily PM_{2.5} concentrations at 1 km resolution in the Eastern United States, *Atmospheric Environment*, 199, 443-452, <https://doi.org/10.1016/j.atmosenv.2018.11.049>, 2019a.
- 680 Goldberg, D. L., Saide, P. E., Lamsal, L. N., de Foy, B., Lu, Z., Woo, J. H., Kim, Y., Kim, J., Gao, M., Carmichael, G., and Streets, D. G.: A top-down assessment using OMI NO₂ suggests an underestimate in the NO_x emissions inventory in Seoul, South Korea, during KORUS-AQ, *Atmos. Chem. Phys.*, 19, 1801-1818, 2019b.



- Good, N., Topping, D. O., Allan, J. D., Flynn, M., Fuentes, E., Irwin, M., Williams, P. I., Coe, H., and McFiggans, G.: Consistency between parameterisations of aerosol hygroscopicity and CCN activity during the RHaMBLe discovery cruise, *Atmos. Chem. Phys.*, 10, 3189-3203, 10.5194/acp-10-3189-2010, 2010.
- 685
- Grell, G., Peckham, S. E., Schmitz, R., McKeen, S. A., Frost, G., Skamarock, W. C., and Eder, B.: Fully coupled “online” chemistry within the WRF model, *Atmospheric Environment*, 39, 6957-6975, 10.1016/j.atmosenv.2005.04.027, 2005.
- Guo, H., Weber, R. J., and Nenes, A.: High levels of ammonia do not raise fine particle pH sufficiently to yield nitrogen oxide-dominated sulfate production, *Scientific Reports*, 7, 12109, 10.1038/s41598-017-11704-0, 2017.
- 690
- Hair, J. W., Hostetler, C. A., Cook, A. L., Harper, D. B., Ferrare, R. A., Mack, T. L., Welch, W., Izquierdo, L. R., and Hovis, F. E.: Airborne High Spectral Resolution Lidar for profiling aerosol optical properties, *Applied Optics*, 47, 6734-6752, 10.1364/ao.47.006734, 2008.
- Hand, J. L., and Kreidenweis, S. M.: A New Method for Retrieving Particle Refractive Index and Effective Density from Aerosol Size Distribution Data, *Aerosol Science and Technology*, 36, 1012-1026, 10.1080/02786820290092276, 2002.
- 695
- Hayes, P. L., Carlton, A. G., Baker, K. R., Ahmadov, R., Washenfelder, R. A., Alvarez, S., Rappenglück, B., Gilman, J. B., Kuster, W. C., de Gouw, J. A., Zotter, P., Prévôt, A. S. H., Szidat, S., Kleindienst, T. E., Offenberg, J. H., Ma, P. K., and Jimenez, J. L.: Modeling the formation and aging of secondary organic aerosols in Los Angeles during CalNex 2010, *Atmos. Chem. Phys.*, 15, 5773-5801, 10.5194/acp-15-5773-2015, 2015.
- Heim, E., Dibb, J., Scheuer, E., Campuzano-Jost, P., Nault, B. A., Jimenez, J. L., Peterson, D., Knote, C., Fenn, M., Hair, J.,
- 700
- Beyersdorf, A. J., Corr, C., and Anderson, B. E.: Asian Dust Observed during KORUS-AQ Facilitates the Uptake and Incorporation of Soluble Pollutants during Transport to South Korea., submitted, 2019.
- Hodzic, A., Chepfer, H., Vautard, R., Chazette, P., Beekmann, M., Bessagnet, B., Chatenet, B., Cuesta, J., Drobinski, P., Goloub, P., Haeffelin, M., and Morille, Y.: Comparison of aerosol chemistry transport model simulations with lidar and Sun photometer observations at a site near Paris, *Journal of Geophysical Research: Atmospheres*, 109, 10.1029/2004jd004735,
- 705
- 2004.
- Hodzic, A., and Jimenez, J. L.: Modeling anthropogenically controlled secondary organic aerosols in a megacity: a simplified framework for global and climate models, *Geosci. Model Dev.*, 4, 901-917, 10.5194/gmd-4-901-2011, 2011.
- Hu, W., Campuzano-Jost, P., Day, D. A., Croteau, P., Canagaratna, M. R., Jayne, J. T., Worsnop, D. R., and Jimenez, J. L.: Evaluation of the new capture vapourizer for aerosol mass spectrometers (AMS) through laboratory studies of inorganic
- 710
- species, 10, 2897-2921, 2017.
- Inness, A., Blechschmidt, A. M., Bouarar, I., Chabrilat, S., Crepulja, M., Engelen, R. J., Eskes, H., Flemming, J., Gaudel, A., Hendrick, F., Huijnen, V., Jones, L., Kapsomenakis, J., Katragkou, E., Keppens, A., Langerock, B., de Mazière, M., Melas, D., Parrington, M., Peuch, V. H., Razinger, M., Richter, A., Schultz, M. G., Suttie, M., Thouret, V., Vrekoussis, M., Wagner, A., and Zerefos, C.: Data assimilation of satellite retrieved ozone, carbon monoxide and nitrogen dioxide with
- 715
- ECMWF's Composition-IFS, *Atmos. Chem. Phys. Discuss.*, 15, 4265-4331, 10.5194/acpd-15-4265-2015, 2015.



- Jimenez, P. A., Hacker, J. P., Dudhia, J., Haupt, S. E., Ruiz-Arias, J. A., Gueymard, C. A., Thompson, G., Eidhammer, T., and Deng, A.: WRF-Solar: Description and Clear-Sky Assessment of an Augmented NWP Model for Solar Power Prediction, *Bulletin of the American Meteorological Society*, 97, 1249-1264, 10.1175/bams-d-14-00279.1, 2016.
- Kabata-Pendias, A., and Pendias, H.: Trace elements in soils and plants, CRC Prees0849315751, 2001.
- 720 Knote, C., Hodzic, A., and Jimenez, J. L.: The effect of dry and wet deposition of condensable vapors on secondary organic aerosols concentrations over the continental US, *Atmos. Chem. Phys.*, 15, 1-18, 10.5194/acp-15-1-2015, 2015.
- Kok, J. F.: A scaling theory for the size distribution of emitted dust aerosols suggests climate models underestimate the size of the global dust cycle, *Proceedings of the National Academy of Sciences*, 108, 1016-1021, 10.1073/pnas.1014798108, 2011.
- 725 Kumar, R., Delle Monache, L., Bresch, J., Saide, P. E., Tang, Y., Liu, Z., da Silva, A. M., Alessandrini, S., Pfister, G., Edwards, D., Lee, P., and Djalalova, I.: Toward Improving Short-Term Predictions of Fine Particulate Matter Over the United States Via Assimilation of Satellite Aerosol Optical Depth Retrievals, *Journal of Geophysical Research: Atmospheres*, 124, 2753-2773, 2019.
- Kupc, A., Williamson, C., Wagner, N. L., Richardson, M., and Brock, C. A.: Modification, calibration, and performance of
730 the Ultra-High Sensitivity Aerosol Spectrometer for particle size distribution and volatility measurements during the Atmospheric Tomography Mission (ATom) airborne campaign, *Atmos. Meas. Tech.*, 11, 369-383, 10.5194/amt-11-369-2018, 2018.
- Kuwata, M., Zorn, S. R., and Martin, S. T.: Using Elemental Ratios to Predict the Density of Organic Material Composed of Carbon, Hydrogen, and Oxygen, *Environmental Science & Technology*, 46, 787-794, 10.1021/es202525q, 2012.
- 735 Lamb, K. D., Perring, A. E., Samset, B., Peterson, D., Davis, S., Anderson, B. E., Beyersdorf, A., Blake, D. R., Campuzano-Jost, P., Corr, C. A., Diskin, G. S., Kondo, Y., Moteki, N., Nault, B. A., Oh, J., Park, M., Pusede, S. E., Simpson, I. J., Thornhill, K. L., Wisthaler, A., and Schwarz, J. P.: Estimating Source Region Influences on Black Carbon Abundance, Microphysics, and Radiative Effect Observed Over South Korea, *Journal of Geophysical Research: Atmospheres*, 123, 13,527-513,548, 10.1029/2018jd029257, 2018.
- 740 Lee, H. H., Bar-Or, R. Z., and Wang, C.: Biomass Burning Aerosols and the Low Visibility Events in Southeast Asia, *Atmos. Chem. Phys. Discuss.*, 2016, 1-55, 10.5194/acp-2016-504, 2016a.
- Lee, S., Song, C. H., Park, R. S., Park, M. E., Han, K. M., Kim, J., Choi, M., Ghim, Y. S., and Woo, J. H.: GIST-PM-Asia v1: development of a numerical system to improve particulate matter forecasts in South Korea using geostationary satellite-retrieved aerosol optical data over Northeast Asia, *Geosci. Model Dev.*, 9, 17-39, 10.5194/gmd-9-17-2016, 2016b.
- 745 Lennartson, E. M., Wang, J., Gu, J., Castro Garcia, L., Ge, C., Gao, M., Choi, M., Saide, P. E., Carmichael, G. R., Kim, J., and Janz, S. J.: Diurnal variation of aerosol optical depth and PM_{2.5} in South Korea: a synthesis from AERONET, satellite (GOCI), KORUS-AQ observation, and the WRF-Chem model, *Atmos. Chem. Phys.*, 18, 15125-15144, 2018.



- Levin, E. J. T., Prenni, A. J., Palm, B. B., Day, D. A., Campuzano-Jost, P., Winkler, P. M., Kreidenweis, S. M., DeMott, P. J., Jimenez, J. L., and Smith, J. N.: Size-resolved aerosol composition and its link to hygroscopicity at a forested site in Colorado, *Atmos. Chem. Phys.*, 14, 2657-2667, 10.5194/acp-14-2657-2014, 2014.
- Liu, X., Huey, L. G., Yokelson, R. J., Selimovic, V., Simpson, I. J., Müller, M., Jimenez, J. L., Campuzano-Jost, P., Beyersdorf, A. J., Blake, D. R., Butterfield, Z., Choi, Y., Crouse, J. D., Day, D. A., Diskin, G. S., Dubey, M. K., Fortner, E., Hanisco, T. F., Hu, W., King, L. E., Kleinman, L., Meinardi, S., Mikoviny, T., Onasch, T. B., Palm, B. B., Peischl, J., Pollack, I. B., Ryerson, T. B., Sachse, G. W., Sedlacek, A. J., Shilling, J. E., Springston, S., St. Clair, J. M., Tanner, D. J., Teng, A. P., Wennberg, P. O., Wisthaler, A., and Wolfe, G. M.: Airborne measurements of western U.S. wildfire emissions: Comparison with prescribed burning and air quality implications, *Journal of Geophysical Research: Atmospheres*, 122, 6108-6129, 2017.
- Liu, Y., Paciorek, C. J., and Koutrakis, P.: Estimating Regional Spatial and Temporal Variability of PM_{2.5} Concentrations Using Satellite Data, Meteorology, and Land Use Information, *Environmental Health Perspectives*, 117, 887, 2009.
- Lu, Z., Streets, D. G., Winijkul, E., Yan, F., Chen, Y., Bond, T. C., Feng, Y., Dubey, M. K., Liu, S., Pinto, J. P., and Carmichael, G. R.: Light Absorption Properties and Radiative Effects of Primary Organic Aerosol Emissions, *Environmental Science & Technology*, 49, 4868-4877, 10.1021/acs.est.5b00211, 2015.
- Mangold, A., De Backer, H., De Paepe, B., Dewitte, S., Chiapello, I., Derimian, Y., Kacenelenbogen, M., Léon, J.-F., Huneus, N., Schulz, M., Ceburnis, D., O'Dowd, C., Flentje, H., Kinne, S., Benedetti, A., Morcrette, J.-J., and Boucher, O.: Aerosol analysis and forecast in the European Centre for Medium-Range Weather Forecasts Integrated Forecast System: 3. Evaluation by means of case studies, *Journal of Geophysical Research: Atmospheres*, 116, 10.1029/2010jd014864, 2011.
- Mätzler, C.: MATLAB functions for Mie scattering and absorption, version 2, IAP Res. Rep., 8, 9, 2002.
- McNaughton, C. S., Clarke, A. D., Howell, S. G., Pinkerton, M., Anderson, B., Thornhill, L., Hudgins, C., Winstead, E., Dibb, J. E., Scheuer, E., and Maring, H.: Results from the DC-8 Inlet Characterization Experiment (DICE): Airborne Versus Surface Sampling of Mineral Dust and Sea Salt Aerosols, *Aerosol Science and Technology*, 41, 136-159, 10.1080/02786820601118406, 2007.
- Mei, F., Hayes, P. L., Ortega, A., Taylor, J. W., Allan, J. D., Gilman, J., Kuster, W., de Gouw, J., Jimenez, J. L., and Wang, J.: Droplet activation properties of organic aerosols observed at an urban site during CalNex-LA, *Journal of Geophysical Research: Atmospheres*, 118, 2903-2917, 10.1002/jgrd.50285, 2013.
- Moise, T., Flores, J. M., and Rudich, Y.: Optical Properties of Secondary Organic Aerosols and Their Changes by Chemical Processes, *Chemical Reviews*, 115, 4400-4439, 10.1021/cr5005259, 2015.
- Myhre, G., Samset, B. H., Schulz, M., Balkanski, Y., Bauer, S., Berntsen, T. K., Bian, H., Bellouin, N., Chin, M., Diehl, T., Easter, R. C., Feichter, J., Ghan, S. J., Hauglustaine, D., Iversen, T., Kinne, S., Kirkevåg, A., Lamarque, J. F., Lin, G., Liu, X., Lund, M. T., Luo, G., Ma, X., van Noije, T., Penner, J. E., Rasch, P. J., Ruiz, A., Seland, Ø., Skeie, R. B., Stier, P., Takemura, T., Tsigaridis, K., Wang, P., Wang, Z., Xu, L., Yu, H., Yu, F., Yoon, J. H., Zhang, K., Zhang, H., and Zhou, C.:



- Radiative forcing of the direct aerosol effect from AeroCom Phase II simulations, *Atmos. Chem. Phys.*, 13, 1853-1877, 10.5194/acp-13-1853-2013, 2013.
- Nault, B. A., Campuzano-Jost, P., Day, D. A., Schroder, J. C., Anderson, B., Beyersdorf, A. J., Blake, D. R., Brune, W. H., Choi, Y., Corr, C. A., de Gouw, J. A., Dibb, J., DiGangi, J. P., Diskin, G. S., Fried, A., Huey, L. G., Kim, M. J., Knote, C. J.,
785 Lamb, K. D., Lee, T., Park, T., Pusede, S. E., Scheuer, E., Thornhill, K. L., Woo, J. H., and Jimenez, J. L.: Secondary organic aerosol production from local emissions dominates the organic aerosol budget over Seoul, South Korea, during KORUS-AQ, *Atmos. Chem. Phys.*, 18, 17769-17800, 10.5194/acp-18-17769-2018, 2018.
- NCEP: NCEP Global Forecast System (GFS) Analyses and Forecasts. <https://doi.org/10.5065/D65Q4TSG>, Research Data Archive at the National Center for Atmospheric Research, Computational and Information Systems Laboratory, Boulder,
790 Colo. Accessed 18 Sept 2019., 2007.
- Peterson, D. A., Hyer, E. J., Han, S.-O., Crawford, J. H., Park, R. J., Holz, R., Kuehn, R. E., Eloranta, E., and Lefer, B. L.: Meteorology Influencing Springtime Air Quality, Pollution Transport, and Visibility in Korea, *Elementa*, under review.
- Petters, M. D., and Kreidenweis, S. M.: A single parameter representation of hygroscopic growth and cloud condensation nucleus activity, *Atmos. Chem. Phys.*, 7, 1961-1971, 10.5194/acp-7-1961-2007, 2007.
- 795 Pfister, G. G., Walters, S., Lamarque, J. F., Fast, J., Barth, M. C., Wong, J., Done, J., Holland, G., and Bruyère, C. L.: Projections of future summertime ozone over the U.S, *Journal of Geophysical Research: Atmospheres*, 119, 5559-5582, 10.1002/2013jd020932, 2014.
- Podolske, J. R., Sachse, G. W., and Diskin, G. S.: Calibration and data retrieval algorithms for the NASA Langley/Ames Diode Laser Hygrometer for the NASA Transport and Chemical Evolution Over the Pacific (TRACE-P) mission, *Journal of*
800 *Geophysical Research: Atmospheres*, 108, 10.1029/2002jd003156, 2003.
- Reddington, C. L., Spracklen, D. V., Artaxo, P., Ridley, D. A., Rizzo, L. V., and Arana, A.: Analysis of particulate emissions from tropical biomass burning using a global aerosol model and long-term surface observations, *Atmos. Chem. Phys.*, 16, 11083-11106, 10.5194/acp-16-11083-2016, 2016.
- Reddington, C. L., Morgan, W. T., Darbyshire, E., Brito, J., Coe, H., Artaxo, P., Scott, C. E., Marsham, J., and Spracklen, D.
805 V.: Biomass burning aerosol over the Amazon: analysis of aircraft, surface and satellite observations using a global aerosol model, *Atmos. Chem. Phys.*, 19, 9125-9152, 10.5194/acp-19-9125-2019, 2019.
- Saide, P. E., Carmichael, G. R., Liu, Z., Schwartz, C. S., Lin, H. C., da Silva, A. M., and Hyer, E.: Aerosol optical depth assimilation for a size-resolved sectional model: impacts of observationally constrained, multi-wavelength and fine mode retrievals on regional scale forecasts, *Atmos. Chem. Phys. Discuss.*, 13, 12213-12261, 10.5194/acpd-13-12213-2013, 2013.
- 810 Saide, P. E., Kim, J., Song, C. H., Choi, M., Cheng, Y., and Carmichael, G. R.: Assimilation of next generation geostationary aerosol optical depth retrievals to improve air quality simulations, *Geophysical research letters*, 41, 2014GL062089, 10.1002/2014gl062089, 2014.



- Schroedter-Homscheidt, M., Oumbe, A., Benedetti, A., and Morcrette, J.-J.: Aerosols for Concentrating Solar Electricity Production Forecasts: Requirement Quantification and ECMWF/MACC Aerosol Forecast Assessment, *Bulletin of the American Meteorological Society*, 94, 903-914, 10.1175/BAMS-D-11-00259.1, 2013.
- Seinfeld, J. H., and Pandis, S. N.: *Atmospheric chemistry and physics: from air pollution to climate change*, John Wiley & Sons, 2016.
- Shah, V., Jaeglé, L., Jimenez, J. L., Schroder, J. C., Campuzano-Jost, P., Campos, T. L., Reeves, J. M., Stell, M., Brown, S. S., Lee, B. H., Lopez-Hilfiker, F. D., and Thornton, J. A.: Widespread Pollution From Secondary Sources of Organic Aerosols During Winter in the Northeastern United States, *Geophysical Research Letters*, 46, 2974-2983, 10.1029/2018gl081530, 2019.
- Shingler, T., Crosbie, E., Ortega, A., Shiraiwa, M., Zuend, A., Beyersdorf, A., Ziemba, L., Anderson, B., Thornhill, L., Perring, A. E., Schwarz, J. P., Campuzano-Jost, P., Day, D. A., Jimenez, J. L., Hair, J. W., Mikoviny, T., Wisthaler, A., and Sorooshian, A.: Airborne characterization of subsaturated aerosol hygroscopicity and dry refractive index from the surface to 6.5 km during the SEAC4RS campaign, *Journal of Geophysical Research: Atmospheres*, 121, 4188-4210, 10.1002/2015jd024498, 2016.
- Shrivastava, M., Fast, J., Easter, R., Gustafson Jr, W. I., Zaveri, R. A., Jimenez, J. L., Saide, P., and Hodzic, A.: Modeling organic aerosols in a megacity: comparison of simple and complex representations of the volatility basis set approach, *Atmos. Chem. Phys.*, 11, 6639-6662, 10.5194/acp-11-6639-2011, 2011.
- Shrivastava, M., Berg, L. K., Fast, J. D., Easter, R. C., Laskin, A., Chapman, E. G., Gustafson, W. I., Liu, Y., and Berkowitz, C. M.: Modeling aerosols and their interactions with shallow cumuli during the 2007 CHAPS field study, *Journal of Geophysical Research: Atmospheres*, 118, 1343-1360, 10.1029/2012jd018218, 2013.
- Skamarock, W. C., Klemp, J. B., Dudhia, J., Gill, D. O., Barker, D. M., Duda, M. G., Huang, X.-Y., Wang, W., and Powers, J. G.: A description of the Advanced Research WRF version 3, NCAR Tech. Note NCAR/TN-475+ STR, 2008.
- Song, S., Gao, M., Xu, W., Shao, J., Shi, G., Wang, S., Wang, Y., Sun, Y., and McElroy, M. B.: Fine-particle pH for Beijing winter haze as inferred from different thermodynamic equilibrium models, *Atmos. Chem. Phys.*, 18, 7423-7438, 10.5194/acp-18-7423-2018, 2018.
- Stier, P., Schutgens, N. A. J., Bellouin, N., Bian, H., Boucher, O., Chin, M., Ghan, S., Huneeus, N., Kinne, S., Lin, G., Ma, X., Myhre, G., Penner, J. E., Randles, C. A., Samset, B., Schulz, M., Takemura, T., Yu, F., Yu, H., and Zhou, C.: Host model uncertainties in aerosol radiative forcing estimates: results from the AeroCom Prescribed intercomparison study, *Atmos. Chem. Phys.*, 13, 3245-3270, 10.5194/acp-13-3245-2013, 2013.
- Tang, H., Zhao, L., Sun, W., Hu, Y., Ji, X., Han, H., and Guan, Q.: Extraction of rubidium from respirable sintering dust, *Hydrometallurgy*, 175, 144-149, <https://doi.org/10.1016/j.hydromet.2017.11.003>, 2018.
- Tang, I. N.: Chemical and size effects of hygroscopic aerosols on light scattering coefficients, *Journal of Geophysical Research: Atmospheres*, 101, 19245-19250, 10.1029/96jd03003, 1996.



- Tuccella, P., Curci, G., Grell, G. A., Visconti, G., Crumeyrolle, S., Schwarzenboeck, A., and Mensah, A. A.: A new chemistry option in WRF-Chem v. 3.4 for the simulation of direct and indirect aerosol effects using VBS: evaluation against IMPACT-EUCAARI data, *Geosci. Model Dev.*, 8, 2749-2776, 10.5194/gmd-8-2749-2015, 2015.
- van Donkelaar, A., Martin, R. V., Brauer, M., Hsu, N. C., Kahn, R. A., Levy, R. C., Lyapustin, A., Sayer, A. M., and
850 Winker, D. M.: Global Estimates of Fine Particulate Matter using a Combined Geophysical-Statistical Method with Information from Satellites, Models, and Monitors, *Environmental Science & Technology*, 50, 3762-3772, 10.1021/acs.est.5b05833, 2016.
- Wang, J., Cubison, M. J., Aiken, A. C., Jimenez, J. L., and Collins, D. R.: The importance of aerosol mixing state and size-resolved composition on CCN concentration and the variation of the importance with atmospheric aging of aerosols, *Atmos. Chem. Phys.*, 10, 7267-7283, 10.5194/acp-10-7267-2010, 2010.
855
- Winijkul, E., Yan, F., Lu, Z., Streets, D. G., Bond, T. C., and Zhao, Y.: Size-resolved global emission inventory of primary particulate matter from energy-related combustion sources, *Atmospheric Environment*, 107, 137-147, 10.1016/j.atmosenv.2015.02.037, 2015.
- Zaveri, R. A., and Peters, L. K.: A new lumped structure photochemical mechanism for large-scale applications, *Journal of Geophysical Research*, 104, 30387-30330,30415, 1999.
860
- Zaveri, R. A., Easter, R. C., Fast, J. D., and Peters, L. K.: Model for simulating aerosol interactions and chemistry (MOSAIC), *J. Geophys. Res.*, 113, D13204, 2008.
- Zhang, X., Turpin, B. J., McMurry, P. H., Hering, S. V., and Stolzenburg, M. R.: Mie Theory Evaluation of Species Contributions to 1990 Wintertime Visibility Reduction in the Grand Canyon, *Air & Waste*, 44, 153-162,
865 10.1080/1073161X.1994.10467244, 1994.
- Zieger, P., Fierz-Schmidhauser, R., Weingartner, E., and Baltensperger, U.: Effects of relative humidity on aerosol light scattering: results from different European sites, *Atmos. Chem. Phys.*, 13, 10609-10631, 10.5194/acp-13-10609-2013, 2013.
- Ziomba, L. D., Lee Thornhill, K., Ferrare, R., Barrick, J., Beyersdorf, A. J., Chen, G., Crumeyrolle, S. N., Hair, J., Hostetler, C., Hudgins, C., Obland, M., Rogers, R., Scarino, A. J., Winstead, E. L., and Anderson, B. E.: Airborne observations of
870 aerosol extinction by in situ and remote-sensing techniques: Evaluation of particle hygroscopicity, *Geophysical research letters*, 40, 417-422, 10.1029/2012gl054428, 2013.



Tables

Table 1. Summary of WRF-Chem simulations. Refractive indices, hygroscopicity parameters and size bins are defined in Table 2 and 3. Refer to section 3.2 and 3.3 for definitions on base and updated configurations.

Name	Aerosol Scheme	Size bins used for OP	GSD of the modes	Refractive index	Hygroscopicity
MOSAIC4b	Sectional 4 bins	4 bins	-	Base	Base
MOSAIC8b	Sectional 8 bins	8 bins	-	Base	Base
RACM1	Modal	8 bins	Base	Base	Base
RACM2	Modal	8 bins	Updated	Base	Base
RACM3	Modal	8 bins	Updated	Updated	Base
RACM4	Modal	8 bins	Updated	Updated	Updated

875



Table 2. Real refractive indexes [dimensionless], hygroscopicity parameter [dimensionless] and aerosol density [g/cm³] used in the base and updated configurations. Values that changed in the updated configurations are noted in cursive. Note that measured organic aerosol density was used in the closure studies.

	Real Refractive Index		Hygroscopicity parameter		Density
	base	updated	base	updated	base
ammonium sulfate	1.52	<i>1.527</i>	0.5	<i>0.61</i>	1.8
ammonium nitrate	1.5	<i>1.553</i>	0.5	<i>0.67</i>	1.8
sodium chloride	1.45	1.45	1.16	1.16	2.2
other inorganics	1.55	1.55	0	<i>0.14</i>	2.6
organic aerosol	1.45	<i>1.55</i>	0	<i>0.14</i>	1
black carbon	1.85	1.85	0	0	1
aerosol water	1.33	1.33	-	-	1



Table 3. Lower and upper diameters in μm for the 4, 8 and 16 size bins configurations

4 bin	Lower	Upper	8 bin	Lower	Upper	16 bin	Lower	Upper
Bin 1	0.039	0.156	Bin 1	0.039	0.078	Bin 1	0.039	0.0552
Bin 2	0.156	0.625	Bin 2	0.078	0.156	Bin 2	0.0552	0.078
Bin 3	0.625	2.5	Bin 3	0.156	0.312	Bin 3	0.078	0.11
Bin 4	2.5	10	Bin 4	0.312	0.625	Bin 4	0.11	0.156
			Bin 5	0.625	1.25	Bin 5	0.156	0.221
			Bin 6	1.25	2.5	Bin 6	0.221	0.312
			Bin 7	2.5	5	Bin 7	0.312	0.442
			Bin 8	5	10	Bin 8	0.442	0.625
						Bin 9	0.625	0.884
						Bin 10	0.884	1.25
						Bin 11	1.25	1.77
						Bin 12	1.77	2.5
						Bin 13	2.5	3.54
						Bin 14	3.54	5
						Bin 15	5	7.07
						Bin 16	7.07	10

Table 4. Description of closure cases. Refer to section 3.2 for definitions on base and updated configurations. Size bins are defined in Table 3.

Name	# of size bins	Refractive index	Hygroscopicity
Closure1	4	Base	Base
Closure2	8	Base	Base
Closure3	16	Base	Base
Closure4	16	Updated	Base
Closure5	16	Updated	Updated



Figures

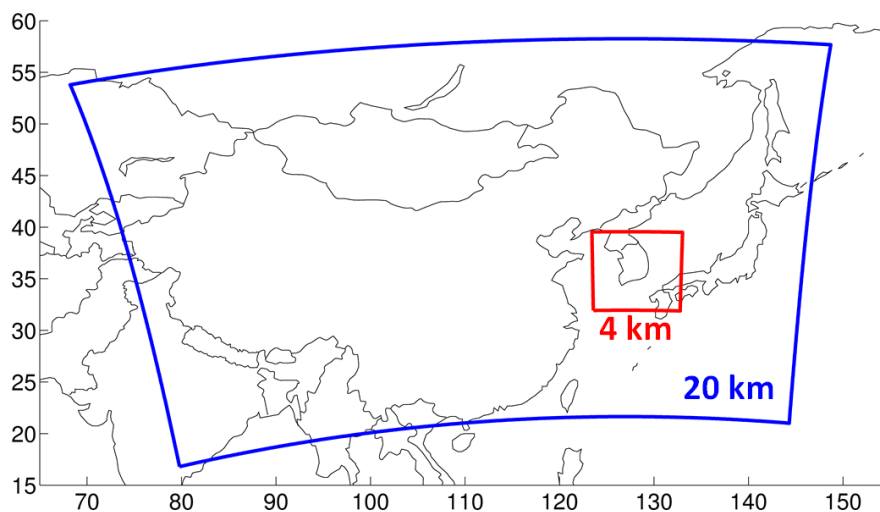
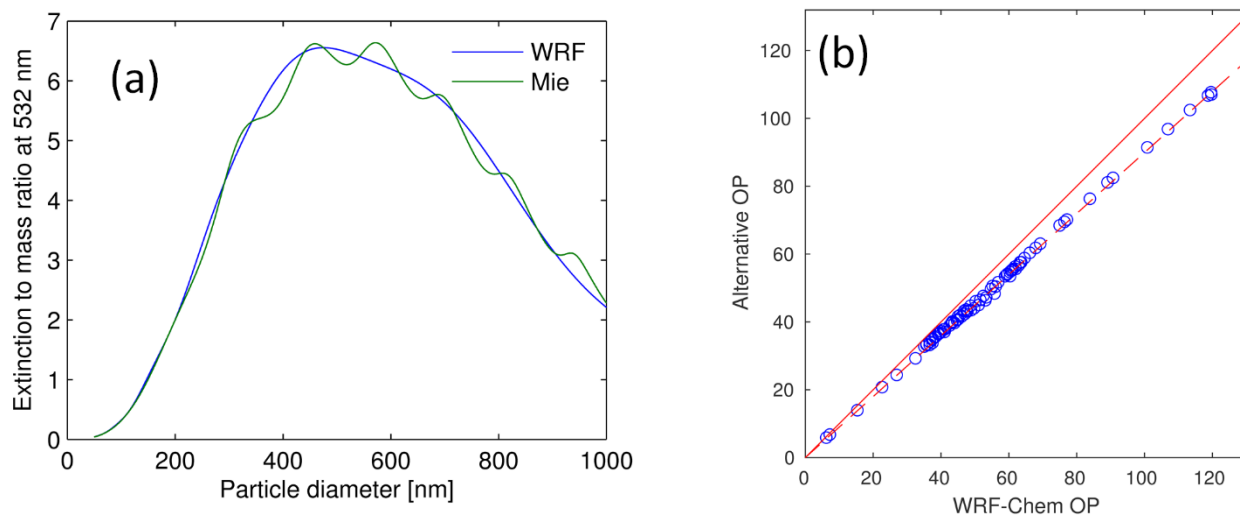


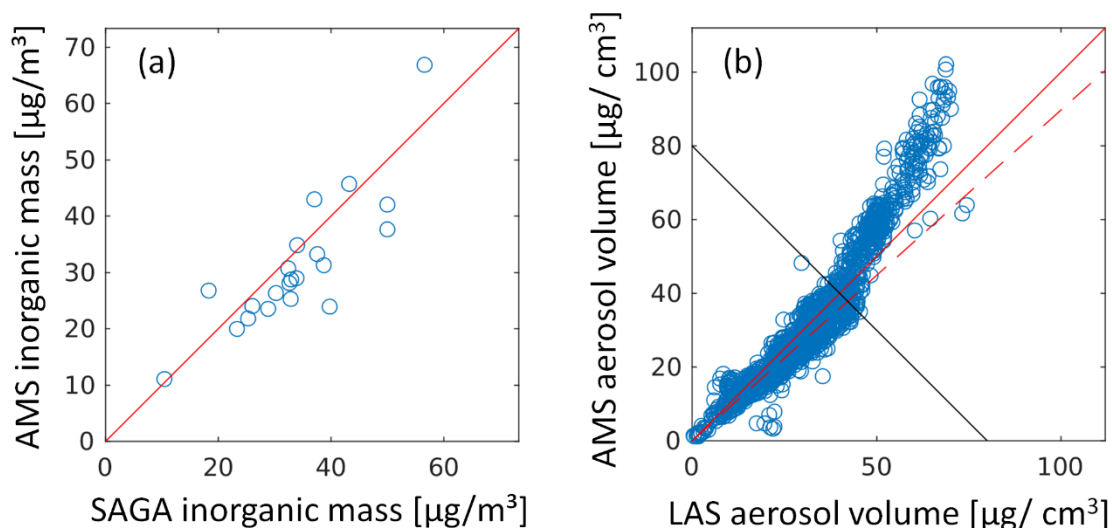
Figure 1. Modeling domains for the forecast simulations. Only the outer domain is used for the retrospective simulations.

890

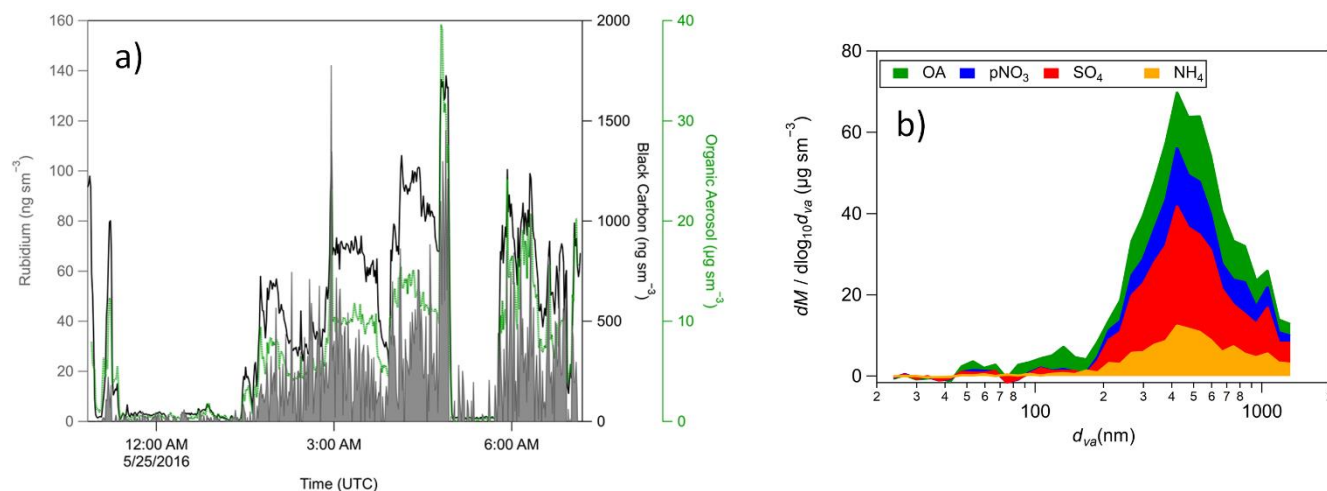


895

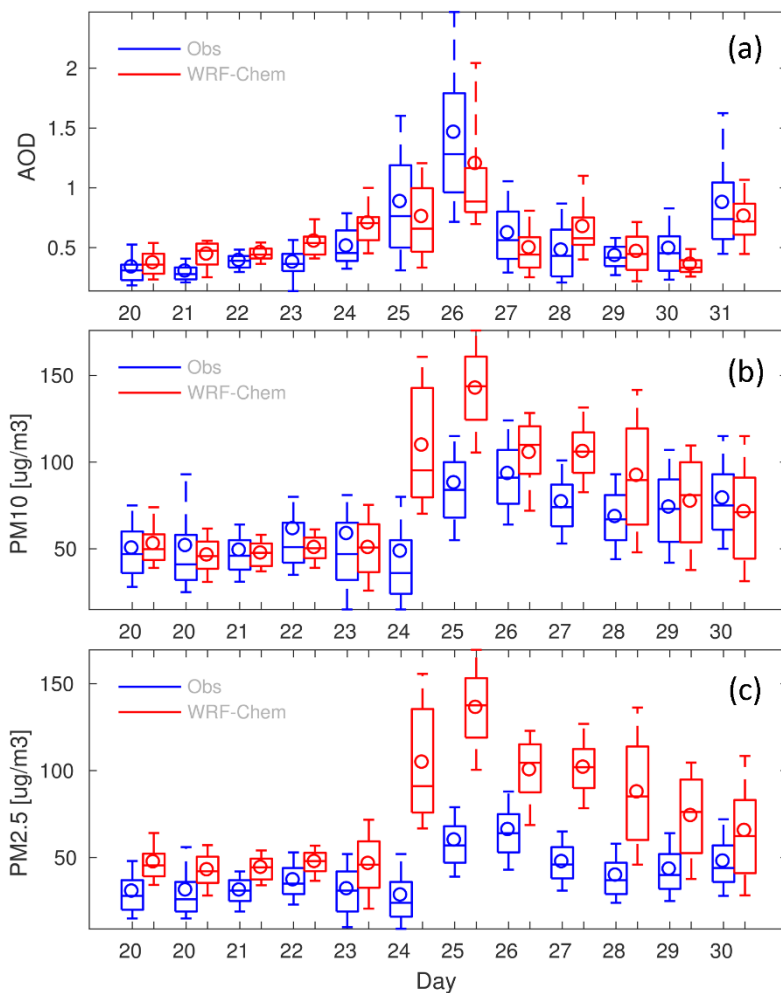
Figure 2. a) Extinction to mass ratio for dry conditions as a function of dry particle diameter considering a monodisperse aerosol distribution of fixed aerosol composition equal to the mean of the data analyzed. Blue and green lines represent results using optical properties code from WRF-Chem and the alternative approach, respectively. b) Scatter plot comparing aerosol water [$\mu\text{g}/\text{m}^3$] estimated by WRF-Chem routines for the forecast simulations (MOSAIC 4 bin) and using the alternative approach. The solid red line indicates the 1:1 line and the dashed red line represents the regression line (slope of 0.9).



900 **Figure 3.** a) Scatterplot of total inorganic aerosol (Sulfate, ammonium, chloride and nitrate) mass [$\mu\text{g}/\text{m}^3$] as measured by SAGA and AMS, averaging the AMS data to the SAGA integration time ($R^2 = 0.72$, slope = 1.07). The solid red line indicates the 1:1 line. b) Scatterplot of aerosol volume measured by the AMS and LAS volume accounting for the AMS transmission. The solid red line indicates the 1:1 line, the solid black line represents an approximate cut-off for the LAS saturation, and the dashed red line represents the regression line when using data below the black line (slope of 0.9).



905 **Figure 4.** a) Time series of rubidium (grey, left axis, measured by the AMS), black carbon (right, black axis, measured by SP2), and total organic aerosol (green, right, measured by AMS), during the haze event sampled by the NASA DC-8 over the Yellow Sea. Rubidium was quantified using the AMS difference signal, a relative ionization efficiency of 1, and the same collection efficiency as the rest of the submicron aerosol (Nault et al., 2018). b) Average size resolved AMS measurements sampled (aerodynamic diameter) by the NASA DC-8 for the same period shown in a).



910

Figure 5. Time series of box and whisker plots for AOD (a), PM10 (b) and PM2.5 (c) for select days on the month of May 2016 comparing observations and forecasts over sites in South Korea. Data are aggregated by day (in UTC time). Center solid lines indicate the median, circles represent the mean, boxes indicate upper and lower quartiles, and whiskers show the upper and lower deciles.

915

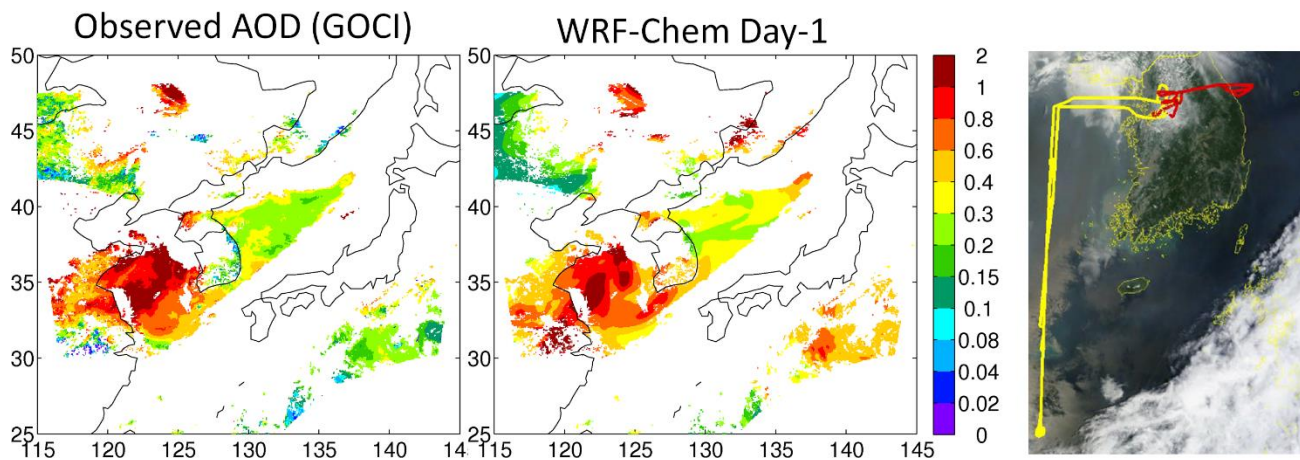


Figure 6. Observed (left) and forecasted (center) AOD maps at 3 UTC (noon local Korean time) on May 25th. The right plot shows Advanced Himawari Imager true color imagery for the same time with overlays of the DC-8 (in yellow) and Twin Otter (in red) flight tracks for that day (Source: KORUS-AQ flight report).

920

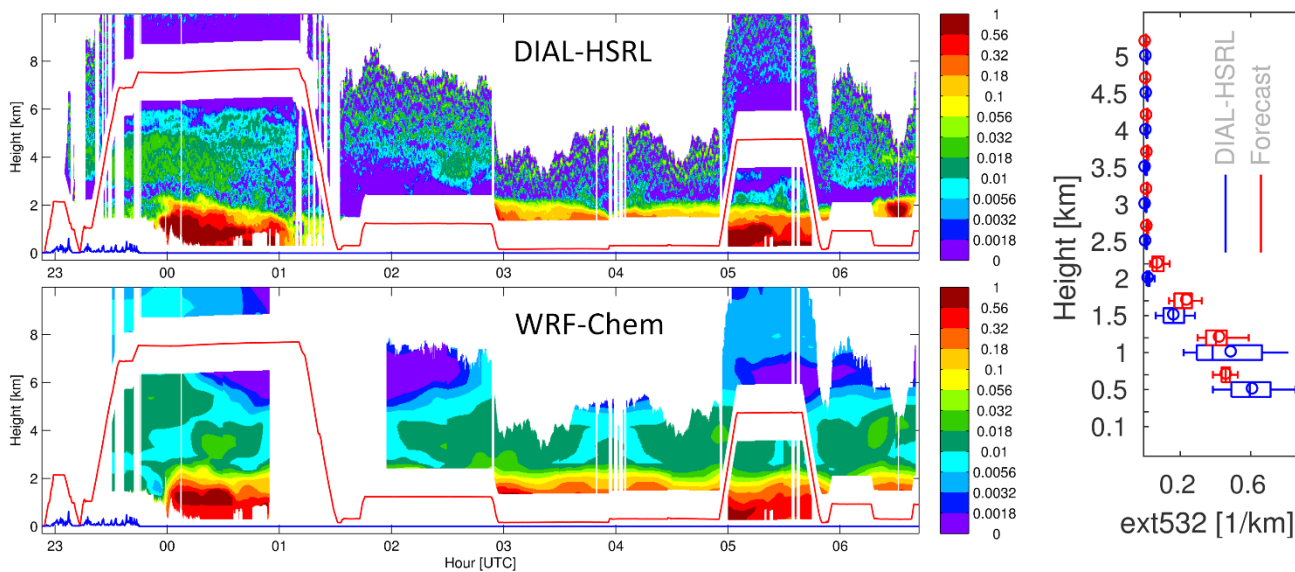
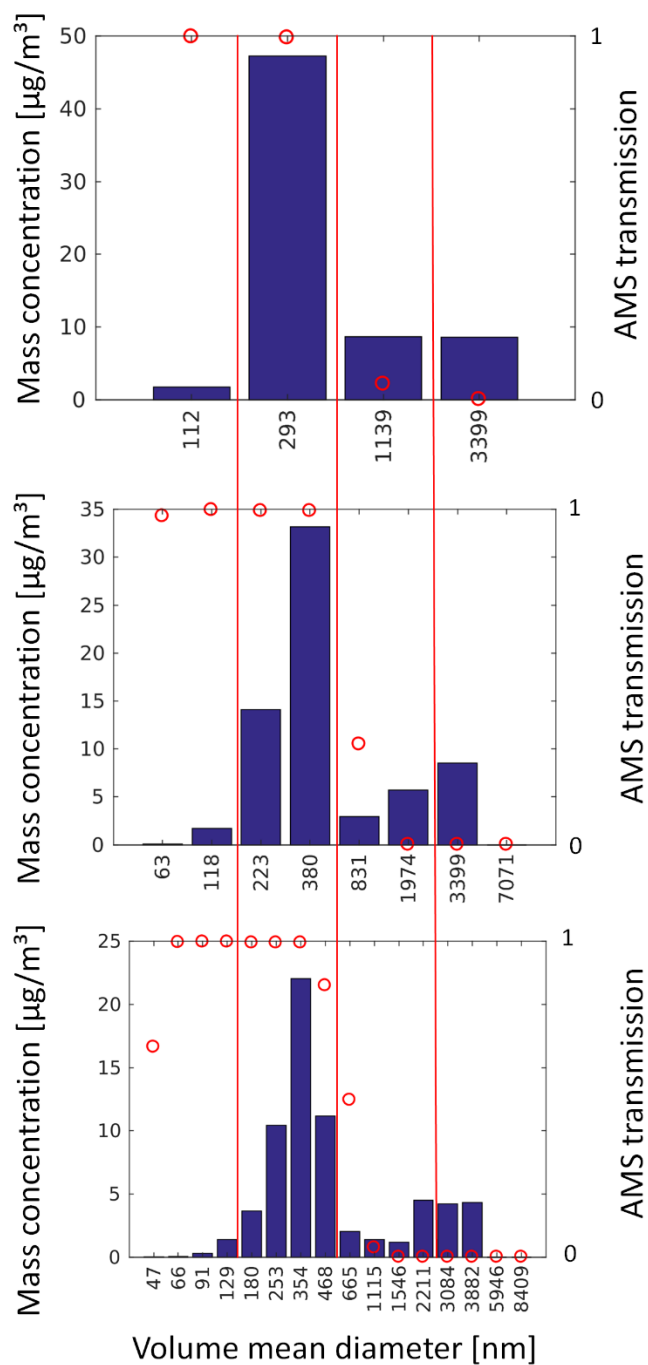
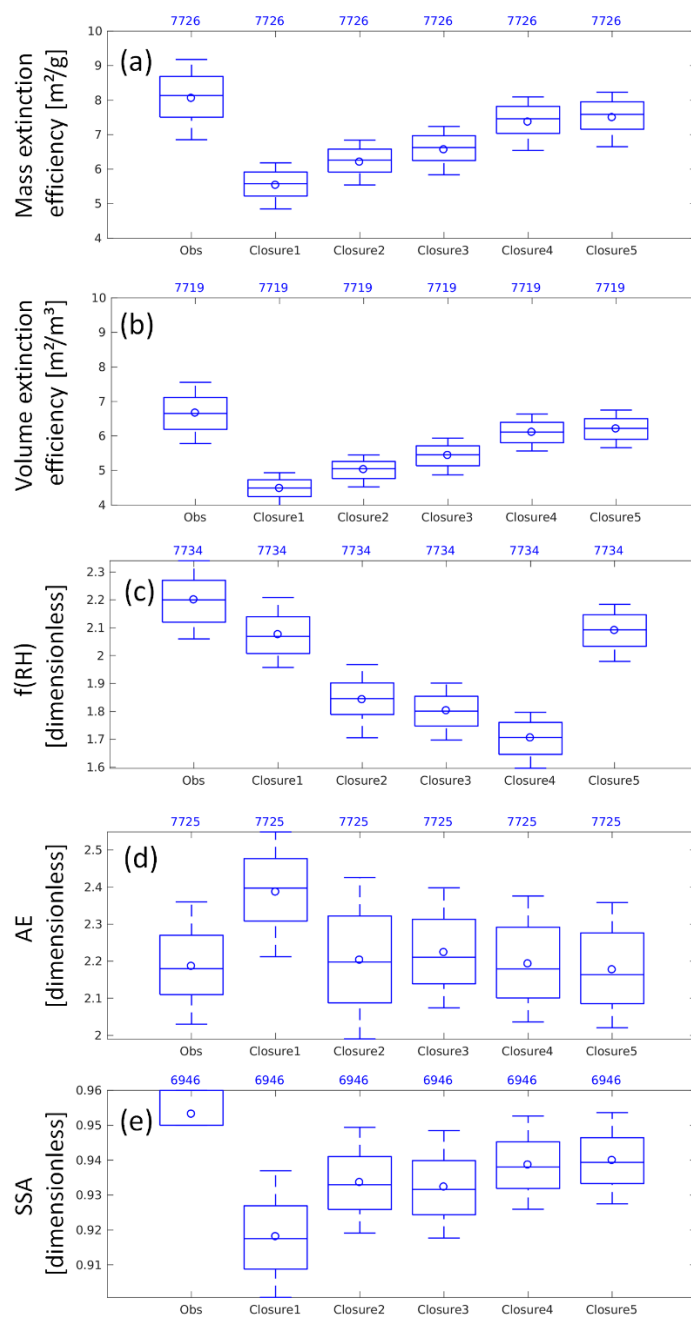


Figure 7. Left panels: DIAL-HSRL (upper panel) and WRF-Chem forecast simulation (bottom panel) extinction curtains at 532 nm for the KORUS-AQ flight on May 24th. Right panel: Box and whisker plots as in Figure 5 aggregating observed and modeled data shown in the left panels for the periods where the aircraft was above the haze layer (00-01 UTC and 5-5:45 UTC).

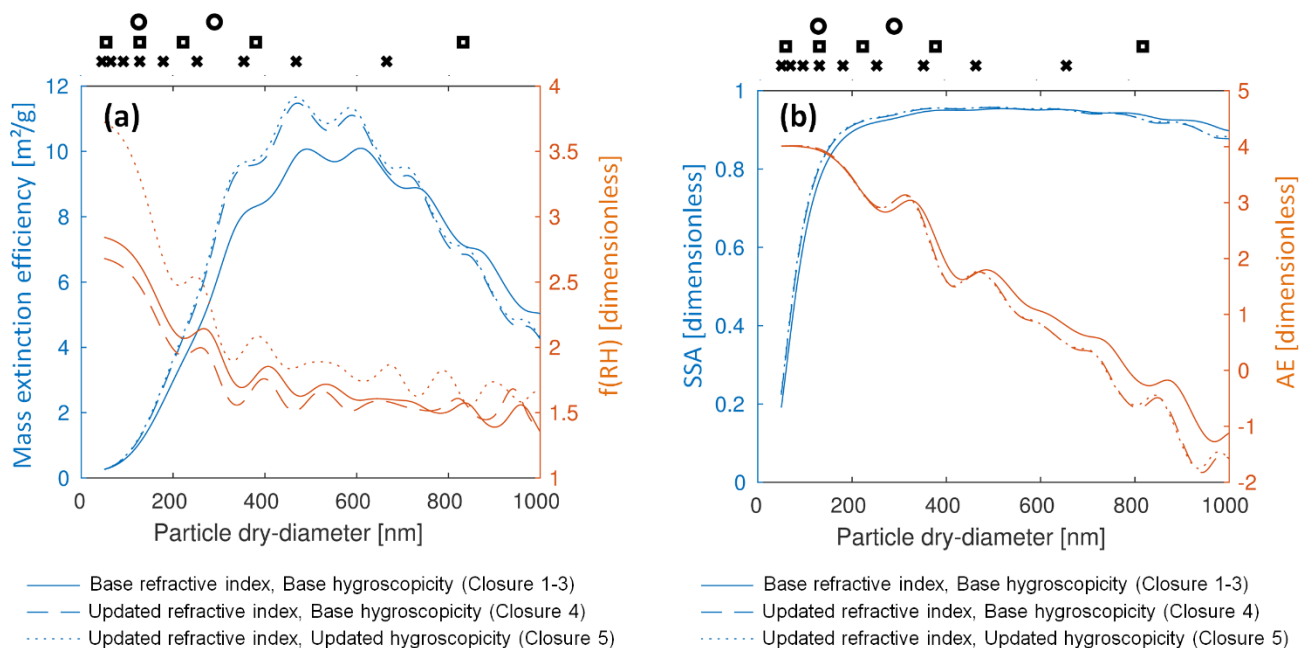
925



930 **Figure 8.** Resulting average size distributions when aggregating observed data (2:00-5:00 UTC) to 4, 8 and 16 size bins. Red lines separate bins aggregated when going from finer to coarser bin representation. Size bins boundaries are defined in Table 3. Red circles indicate the average AMS transmission efficiency (dimensionless) for each size bin.



935 **Figure 9** Box and whisker plots (as in Fig. 5) showing observations and closure results driving the optical properties code with observations. Closure cases are described in Table 4. Results are shown for (a) the extinction (550 nm) to mass ratio (mass extinction efficiency), (b) extinction to volume ratio (volume extinction efficiency), (c) f(RH) measured at 550 nm, (d) 550-700 Angstrom exponent and (e) Dry single-scattering albedo. The blue numbers on top of the plots represent the sample size used when computing statistics.



940 **Figure 10. a) Volume extinction efficiency (blue, scale on the left) and $f(\text{RH})$ (orange, scale on the right) as a function of geometric**
dry particle diameter considering a monodisperse aerosol distribution of fixed aerosol composition equal to the mean of the data
analyzed. Different lines represent cases where real refractive index and hygroscopicity correspond to the base and updated
conditions (see text for details). Black markers on top of the plots represent the calculated volume mean diameter for each size bin
when using 4 (circles), 8 (squares) and 16 (x's) bins for the mean observed size distribution (numerical values found on Fig. 8).
945 **Note only mean diameters below 1 μm are shown. b) Same as a) but for dry Single-scattering albedo and 550-700nm Angstrom**
Exponent.

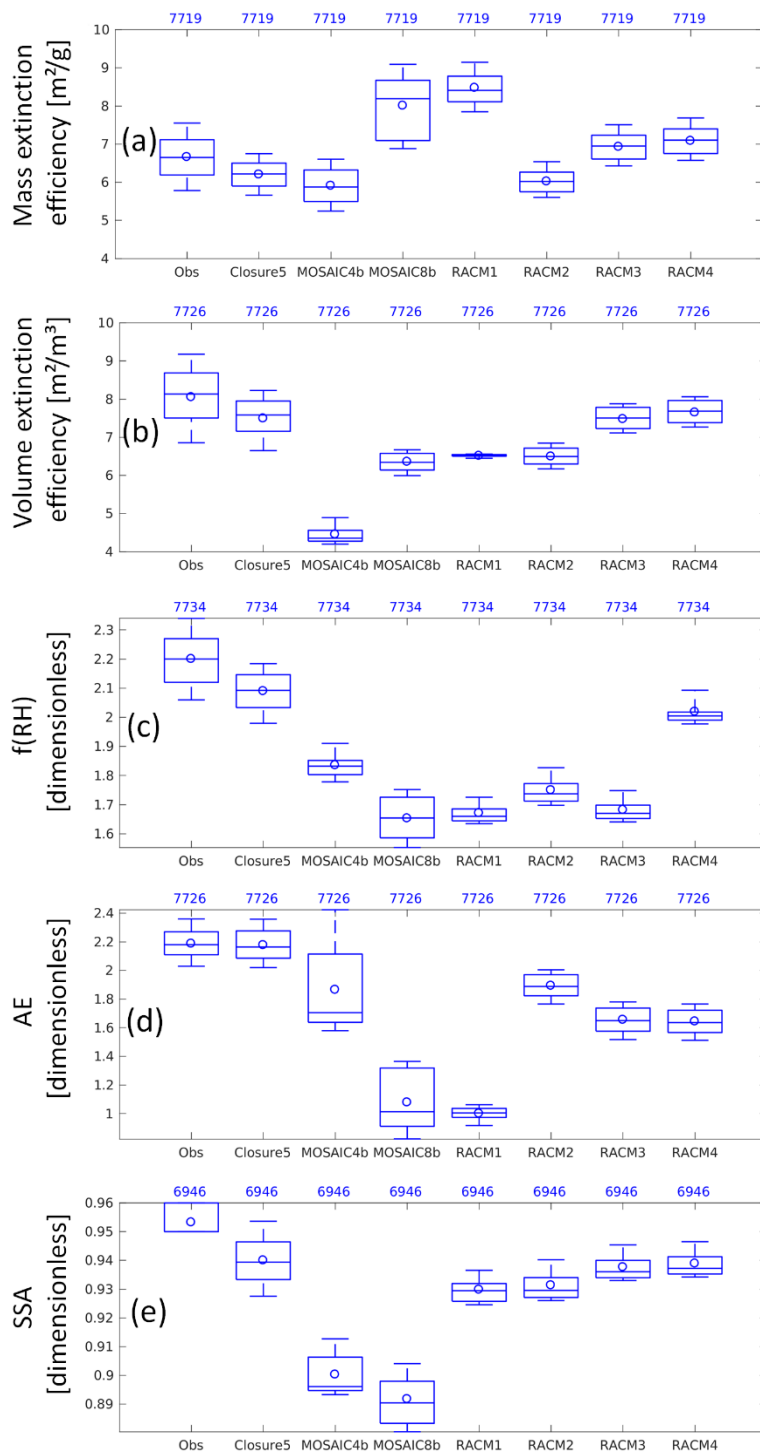
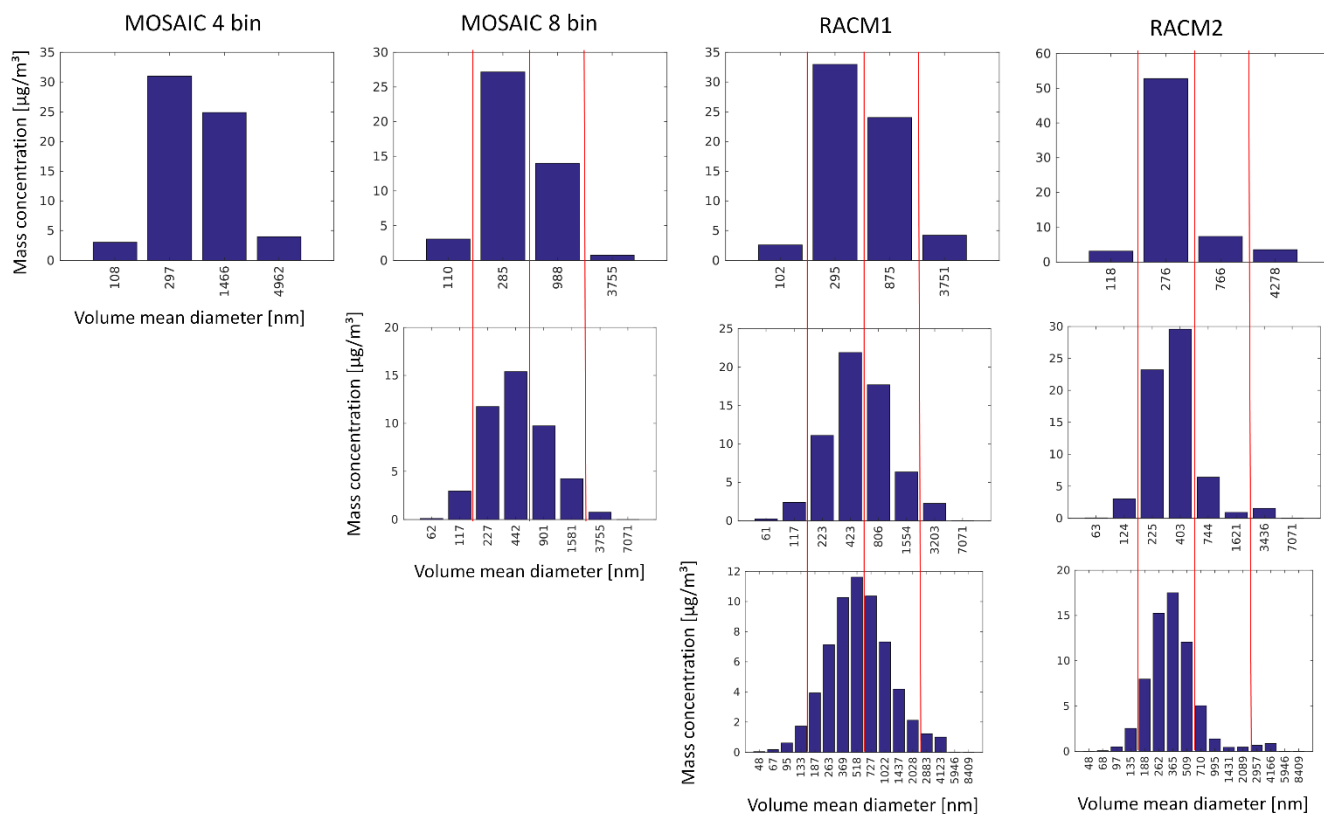
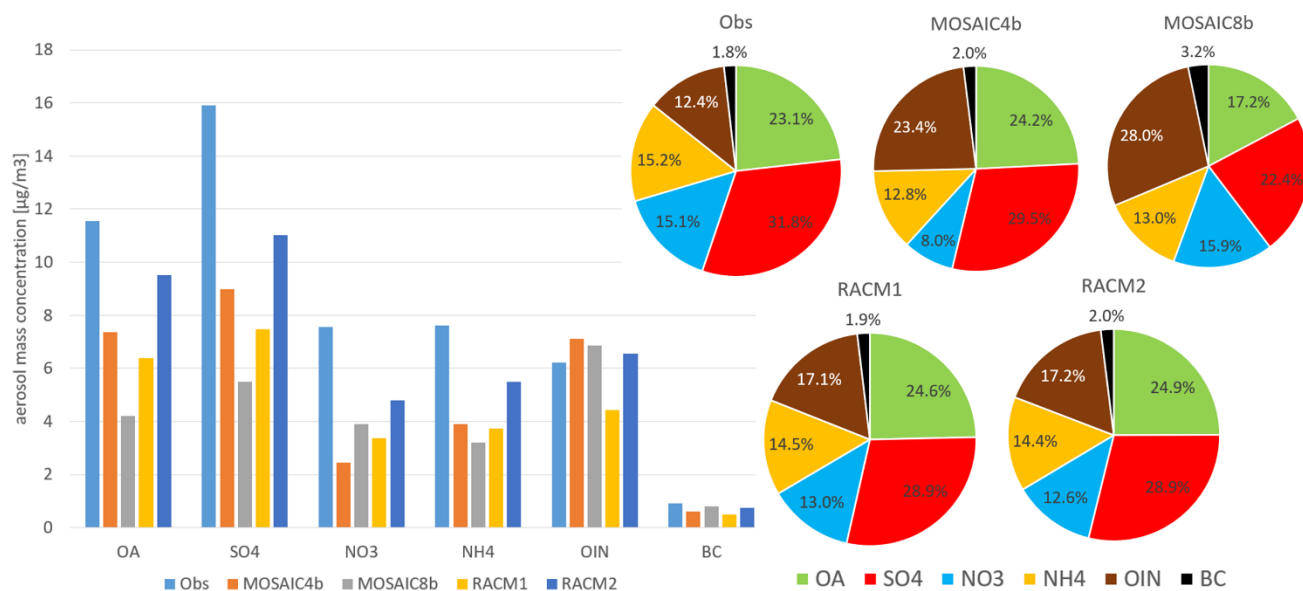


Figure 11. As Figure 9 but comparing observations and Closure study 5 to different modeling configurations (described in Table 1).



950

Figure 12. Same as Figure 8 but for simulations using different modeling configurations. Size bins are aggregated to coarser bins when possible for comparison across configurations. Size bin boundaries are defined in Table 3.



955

Figure 13. Left panel: Bar plot showing sub-micron aerosol mass concentration by species for observations (AMS+SP2) and retrospective simulations. Right panels: Pie charts showing percentage contribution by each species for observations and retrospective simulations.